



From Continental to Street Scales: Climate Change Impacts on Atmospheric Composition over Europe and London

5 Ruth M. Doherty^{1*}, Zhenze Liu^{2,1*}, Massimo Vieno³, Oliver Wild⁴, Fiona M. O' Connor^{5,6}, Steven T. Turnock^{5,7}, Christina M. Hood³, Jenny R. Stocker⁸, Mathew R. Heal⁹, Dwayne E. Heard¹⁰, Emma G. Sands¹, David J. Carruthers⁸, Lisa K. Whalley^{10,11}

¹School of GeoSciences, University of Edinburgh, Edinburgh, EH9 3FF, UK

10 ²School of Environmental Science and Engineering, Nanjing University of Information Science and Technology, Nanjing, China

³UK Centre for Ecology & Hydrology, Bush Estate, Penicuik, Midlothian, EH26 0QB, UK

⁴Lancaster Environment Centre, Lancaster University, Lancaster, LA1 4YQ, UK

⁵Met Office Hadley Centre, Exeter, EX1 3PB, UK

15 ⁶Department of Mathematics and Statistics, Global Systems Institute, University of Exeter, Exeter, EX4 4QJ, UK

⁷Metoffice@Leeds, School of Earth and Environment, University of Leeds, Leeds, LS2 9JT, UK

⁸Cambridge Environmental Research Consultants, Cambridge, CB2 1SJ, UK

⁹School of Chemistry, University of Edinburgh, Edinburgh, EH9 3FJ, UK

¹⁰School of Chemistry, University of Leeds, Leeds, LS2 9JT, UK

¹¹National Center for Atmospheric Science, University of Leeds, Leeds, LS2 9JT

20

Correspondence to: Ruth M. Doherty (ruth.doherty@ed.ac.uk)

Abstract. Climate change will impact ozone (O_3) and fine particulate matter ($PM_{2.5}$) through its influence on natural emissions, atmospheric chemistry, deposition and transport. A coupled modelling approach is employed to identify the key processes and determine how regional air pollution across Europe and urban-scale air quality in London in the 2090s are impacted by climate change under Representative Concentration Pathway (RCP) 8.5. Climate change projections from the HadGEM2-ES Earth System Model nudge the nested WRF-EMEP4UK model, which drives the street-scale ADMS-Urban model. Annual-mean temperature increases exceeding $4^\circ C$ produce substantial increases in summer biogenic isoprene emissions. There is a strong contrast in the summer and winter-mean O_3 responses to climate change, with large summer increases over southern Europe (up to 10 ppbv) and winter decreases over Europe. Annual-average $PM_{2.5}$ concentrations are elevated (5-10 $\mu g m^{-3}$) over most of Europe, also driven by higher summer isoprene emissions that promote secondary organic aerosol formation. Decreases in primary and inorganic $PM_{2.5}$ components are prominent in winter. The seasonality of urban air pollution is modified over London under climate change: the O_3 peak amplitude is reduced, whilst the winter peaks in $PM_{2.5}$ and NO_2 are more pronounced, with nighttime increases. The diurnal profile of urban air pollution typically flattens. Climate induced changes in O_3 aid attainment of long-term air quality guidelines in northern Europe, but pose challenges elsewhere. Achieving long-term $PM_{2.5}$ guidelines over much of Europe becomes increasing difficult with climate change, while attaining short-term air quality guidelines in London remains a major challenge, especially for NO_2 .



1 Introduction

Climate change, even in the absence of anthropogenic emission changes, will influence regional air quality with implications for human and ecosystem health (Silva et al. 2017; Emberson 2020). The impacts of climate change on atmospheric 40 composition and air quality have been widely studied at global and continental scales using coupled chemistry-climate models, Earth System Models (ESMs) or atmospheric chemistry transport models driven by meteorology from global or regional climate models. Many of these studies focus on understanding change in O₃ or PM_{2.5} air quality. Climate change influences both background and local air quality by altering meteorological conditions that affect a) atmospheric chemistry and physical processes b) natural emissions of air pollutant precursors and deposition, and c) long-range transport and 45 mixing processes. These processes are often interconnected; for example, climate change affects vegetation functioning, modifying atmosphere-biosphere interactions.

Previous studies have outlined key effects through the direct impact of meteorological variables on atmospheric chemical kinetics. Over remote regions, higher temperatures lead to more water vapour and greater O₃ destruction resulting in lower surface O₃ background levels (Johnson et al. 1999; Doherty et al. 2013; West et al. 2013; Schnell et al. 2016; Turnock et al. 50 2022). High confidence in this effect was noted in the IPCC 5th Assessment (Kirtman et al. 2013). Higher humidities also enhance hydroxyl radical (OH) abundances leading to greater O₃ formation, but also greater O₃ loss through conversion of NO_x to nitric acid (HNO₃) in polluted regions (Jacob and Winer 2009; Lu et al. 2019). In winter in the midlatitudes, such changes in photochemistry compete with direct titration of O₃ by NO in high NO_x regions (Lacressonnière et al. 2014). Faster thermal decomposition of peroxyacetyl nitrate (PAN) reduces O₃ production in remote regions but increases NO_x in 55 source regions, which typically promotes O₃ formation (Doherty et al. 2013). These processes impact NO_x, O₃ and CH₄ lifetimes leading to further changes in atmospheric chemistry (Thornhill et al. 2021). Schnell et al. (2016) summarises the overall O₃ impact of climate change through warmer temperatures, more water vapor, and faster chemical kinetics, as an increase in the efficiency of precursor emissions to generate surface O₃ in polluted regions, reducing precursor export to neighbouring downwind locations. For surface PM_{2.5}, studies note the important kinetic effects of temperature rise on 60 inorganic and organic aerosol species abundances. Higher temperatures lead to faster oxidation that increases formation of sulphate, and potentially organic aerosol, but reduces the partitioning of nitrate to its condensed phase, decreasing nitrate aerosol loading (Dawson et al. 2007; Pye et al. 2009; Fiore et al. 2012; Doherty et al. 2017).

Changes in climate will impact atmosphere-biosphere interactions. The response of biogenic emissions to climate change remains debated (Langner et al. 2012; Lu et al. 2019; Zanis et al. 2022). Isoprene and monoterpene emissions from 65 vegetation are strongly temperature dependent, but the effect of increasing atmospheric CO₂ concentrations (the CO₂ inhibition effect; Arneth et al. 2008) has been shown to offset a temperature-driven isoprene emissions response. Uncertainties in isoprene nitrate chemistry further complicate understanding of the influence of climate changes on isoprene, the dominant global volatile organic compound (VOC), that strongly influences O₃ levels (Fu and Tian, 2019). Isoprene and monoterpenes are also key secondary organic aerosol (SOA) precursors. Climate-driven isoprene-derived SOA effects have



70 been widely studied (e.g., Lin et al. 2016; Gomez et al. 2023). Fewer studies have considered the sensitivity of monoterpene emissions to climate, but those that have suggest a large temperature-driven response, leading to higher PM_{2.5} through greater SOA abundance (Lin et al. 2016; Turnock et al. 2022; Gomez et al. 2023). Natural primary emissions of coarse sea-salt and dust particles, which partly contribute to PM_{2.5}, respond to climate change through changes in wind speeds and transport patterns and impacts on soil moisture (Thornhill et al. 2021; Turnock et al. 2022); however, the dust response to 75 climate change is highly uncertain (Gomez et al. 2023; Liu et al. 2024). Deposition processes can also be altered under climate change. Climate-driven changes in stomatal functioning and in aerodynamic resistance are likely to suppress O₃ dry deposition in summer (Andersson and Engardt 2010; Vieno et al. 2010). Several studies also highlight increases in surface PM_{2.5} attributed to reduced large-scale precipitation and hence less wet deposition over land (Allen et al. 2016; Allen et al. 2019; Banks et al. 2022).

80 Atmospheric composition and air quality will be impacted by changes in transport and local mixing in response to climate change. Climate induced changes in anticyclone frequency and longevity may drive changes in local stagnation that are associated with air pollutant build-up and in summer. When anticyclonic conditions lead to heatwaves this will modify air pollution levels (Vieno et al. 2010; RS 2021). Enhanced stratosphere-troposphere exchange (STE) of O₃ may also influence surface O₃ (Zeng and Pyle 2003; Young et al. 2013; Zanis et al. 2022).

85 Climate change impacts over Europe have been quantified in a considerable number of studies, most of which have applied global climate models, although a few studies have employed regional models (Andersson and Engardt et al 2010; Colette et al. 2015; Langner et al. 2012; Lacressonnière et al. 2016). For surface O₃, most studies for Europe have focussed on the summer season (either June-July-August or April-September). Colette et al. (2015) performed a meta-analysis of 25 model 90 projections (Special Report on Emissions Scenarios (SRES) and Representative Concentration Pathway (RCP) pathways) with present-day air pollutant emissions, that revealed a latitudinal gradient in the impacts of climate change on surface O₃ in summer over Europe, with reductions over the North Atlantic region and northern Europe and increases over large areas of continental Europe of up to 5 ppbv by 2071-2100, that they associate with the processes described above. The representation of hemispheric background O₃ (influenced by O₃ destruction under climate change) and of isoprene are the main sources of uncertainty in this regional model intercomparison. Subsequent studies have reported consistent spatial patterns and 95 magnitudes of change in surface O₃ in summer across Europe due to climate change in 2100 when using scenarios with a large projected global warming (RCP 8.5 or Shared Socioeconomic Pathways (SSP)3-7.0) (Schnell et al. 2016; Silva et al. 2017; Turnock et al. 2022). Schnell et al. (2016) notes that even with constant biogenic isoprene emissions, some models suggest summer mean O₃ increases in southern Europe under RCP8.5.

100 For PM_{2.5} over Europe, typically the impact of climate change on the annual mean abundance has been analysed. Studies using RCP 8.5 and SSP3-7.0 pathways for climate change in 2100 typically show a latitudinal gradient with small absolute changes of 0-1 µg m⁻³ over northern Europe and more pronounced changes over southern Europe (~3 µg m⁻³). These changes are attributed to elevated biogenic emissions under climate change (Turnock et al. 2020, 2022; Gomez et al. 2023) and less wet deposition arising from reduced large-scale precipitation (Silva et al. 2017). A regional model intercomparison by



105 Lacressonnière et al. (2016) highlights that the response of $PM_{2.5}$ to climate change over Europe depends largely on emissions driven changes in SOA. Meanwhile, changes in precipitation, relative humidity and winds are important drivers for other $PM_{2.5}$ components, with dust representation being a major uncertainty.

110 A small number of studies, using global and regional models, have isolated the impacts of climate change on air quality over the UK. An analysis of model output from the Coupled Model Intercomparison Project (CMIP6) suggests that under the SSP3-7.0 pathway, annual-mean surface O_3 mixing ratios over the UK decrease by 3 ppbv in 2100 due to greater O_3 destruction over the Atlantic (RS, 2021). A meta-analysis by Colette et al. (2015) identified summer mean surface O_3 reductions of up to 3 ppbv under RCP8.5 by the end of the century. At the urban-scale, one study examined climate change effects on air quality over London using a dispersion model driven by outputs from the HadCM3 climate model under the SRES A2 scenario for 2071-2100 (Athanasiadou et al. 2010). Urban annual-average O_3 concentrations increased in the future, while PM_{10} showed little change. However, this study used a simple statistical model to represent background concentrations that neglected the relationship between O_3 and specific humidity. All the processes described above are important at the local-scale. Furthermore, the magnitude of O_3 and $PM_{2.5}$ responses to climate change may vary with model resolution since underlying processes and their representation e.g., of emissions and the resulting chemical regime may be resolution dependent (Zanis et al. 2022).

115 UK Climate Projections 2018 (UKCP18) based on RCP8.5 simulations are available at high resolution through dynamical downscaling of the HadGEM3 model, and include estimates of uncertainty (Murphy et al. 2018). However, there is a lack of high-resolution future projections that include air quality and climate interactions due to the computational expense of incorporating interactive chemistry (Doherty et al. 2022; Fiore et al. 2022) and dynamical downscaling. This study therefore seeks to use multi-scale nested modelling (global to regional to local) to address this issue and capture important processes relevant to the different scales. The need for regional and urban-scale capabilities for future projections is pertinent for the 120 revised 2021 World Health Organisation guidelines. These provide new air quality guidelines and interim targets that are considerably more stringent, and include for the first time peak season O_3 targets and guidelines (WHO 2021). Future emission policies will need to account for the climate change impacts on both background and local O_3 and $PM_{2.5}$ air quality in order to achieve these targets/guidelines. In addition, studies of NO_2 changes driven by climate change in relation to WHO 125 guidelines are absent. Hence the capability to simulate regional and street-scale atmospheric composition together using a consistent approach that identifies the key driving processes is a pressing requirement.

130 The aim of this study is therefore to employ a consistent nested global-regional-urban scale modelling system to investigate how substantial future changes in climate may impact continental, regional and urban-scale atmospheric composition over Europe, the UK and London, focussing on the key drivers at different spatial and temporal scales, and the implications for meeting WHO air quality guidelines. The nested modelling approach and simulations performed are described in Sect. 2. 135 Climate change impacts on atmospheric composition over Europe are discussed in Sect. 3, focusing on surface O_3 and $PM_{2.5}$ and its components and investigating the key driving processes. Climate-change driven changes in seasonal variability of surface O_3 , $PM_{2.5}$ and for the first time NO_2 are examined for the UK and London as well as the change in diurnal cycles



over the UK in Sect. 4. The influence of climate change for achieving WHO (2021) air quality interim targets and guidelines for O₃, PM_{2.5} and NO₂ are explored in Sect. 5. Conclusions are presented in Sect. 6.

140 2 Methods

A multi-scale nested modelling approach, which couples regional and urban-scale processes, is employed in this study. The modelling framework integrates a regional atmospheric chemistry transport model, a local dispersion model, and a numerical weather prediction model, driven by global change climate projections from an Earth System Model. Details of each model and the coupling chain are presented in the following sections.

145 2.1 Global-scale climate modelling

The global model used to provide climate change projections in this study, is the HadGEM2-ES Earth System Model (Collins et al. 2011). HadGEM2-ES is a coupled atmosphere-ocean model, with additional Earth system components such as dynamic vegetation, interactive chemistry and aerosols, and a terrestrial and ocean carbon cycle (Collins et al., 2011). HadGEM2-ES was used extensively to contribute model outputs from ensembles of historical and future simulations to 150 Phase 5 of the Coupled Model Intercomparison Project (CMIP5; Taylor et al., 2012). Further details on the implementation of forcings for all CMIP5 simulations are provided in Jones et al. (2011). 3-D distributions of temperature, specific humidity, U and V wind components, surface pressure, soil temperature and moisture from HadGEM2-ES were used as initial and 6-hourly boundary conditions for nested regional numerical weather prediction simulations described below (Sect. 2.2).

2.2 Regional-scale modelling

155 The EMEP4UK model is based on the European Monitoring and Evaluation Programme Meteorological Synthesizing Centre-West (EMEP MSC-W) chemistry transport model, used by the UNECE Convention on Long-range Transboundary Air Pollution to assess trans-boundary air pollution in Europe. The EMEP4UK model version applied in this study to simulate regional atmospheric composition and air quality metrics is based on EMEP MSC-W rv4.6 (Simpson et al. 2012, 2015). It uses a one-way nested approach with two domains: an outer domain covering the majority of Europe which 160 provides boundary conditions for a UK nested domain (Vieno et al. 2010, 2014, 2016). The EMEP4UK model meteorological driver is the WRF model version 3.6.1 (www.wrf-model.org). In addition to using initial and 6-hourly lateral boundary conditions from HadGEM2-ES, WRF simulations are nudged every 6 hours in 3-D, using temperature and U and V wind components from HadGEM2-ES.

The EMEP4UK and WRF models use the same grid definition, with a horizontal resolution of 50 km × 50 km for the 165 European domain and 5 km × 5 km for the UK domain. An intermediate domain with 10 km × 10 km horizontal resolution is also used for WRF. The models also share the same vertical grid that employs 21 vertical levels from the surface to 100 hPa,



with the lowest vertical layer ~50 m deep. Modelled air pollutant concentrations described here as surface concentrations have been adjusted to correspond to 3 m above the surface (Simpson et al., 2012).

EMEP4UK uses the CRI-v2-R5 gaseous chemical mechanism (Watson et al., 2008), which has 220 species and 609 reactions. Five classes of fine and coarse particles are represented in EMEP4UK. Gas–aerosol partitioning of secondary inorganic aerosol utilises the Model for an Aerosol Reacting System (MARS) equilibrium module (Simpson et al., 2012); secondary organic aerosol formation uses the volatility basis set approach (Bergström et al., 2012). $PM_{2.5}$ is the sum of fine ammonium (NH_4^+), sulphate (SO_4^{2-}), fine nitrate (NO_3^-), fine elemental carbon (EC), fine organic matter (OM), fine sea salt (SS), fine mineral dust, and 27 % of the coarse nitrate aerosol (Vieno et al. 2016). The WRF-EMEP4UK nested model system used here has been thoroughly evaluated against measurements (Vieno et al. 2010; Ots et al. 2016, Lin et al. 2017), including provision of evidence on air quality to the UK government (e.g., AQEG, 2021).

Anthropogenic and greenhouse gas emissions are annually invariant to permit a clearer isolation of the climate change signal. Anthropogenic emissions of NO_x , NH_3 , SO_2 , primary $PM_{2.5}$, primary coarse PM ($PM_{2.5-10}$), CO and non-methane VOCs) for 2012 are derived from the EMEP Centre for Emission Inventories and Projections (CEIP, www.ceip.at, last access: 1 August 2018). The National Atmospheric Emission Inventory (NAEI, <http://naei.defra.gov.uk>) is used for anthropogenic emissions for the UK for 2012 at 1 km resolution. Shipping emission estimates for the UK domain are derived from ENTEC (2010), projected to 2012. Annual total anthropogenic emissions derived from the inventories are resolved to hourly resolution using prescribed monthly, day-of-week and diurnal hourly emissions factors and distributed vertically (Simpson et al., 2012).

Biogenic emissions of isoprene and monoterpene (α -pinene) in EMEP4UK are calculated interactively using surface temperature and insolation (Guenther et al., 1995; Simpson et al. 2012) and therefore respond to the changes in climate as simulated in these nudged WRF simulations. CO_2 inhibition of isoprene emission (Arneth et al. 2008) is not included in this EMEP4UK model version. Emissions of NO_x from soils, which are temperature dependent, and of wind-driven sea salt are also calculated interactively (Simpson et al. 2012). Other natural emissions (lightning, DMS, Saharan dust, volcanic) are fixed and hence invariant between the present-day and future coupled model simulations. Lightning NO_x emissions are prescribed here but interactive schemes used in other studies have shown strong responses to climate change, although not over Europe (Finney et al. 2018). In the standard EMEP4UK set-up biomass burning emissions are prescribed annually. To avoid introducing interannual variability in biomass burning emissions, these emissions were turned off altogether. The import of Saharan dust is treated using a monthly dust climatology.

Longer lived gaseous species are provided as boundary and initial conditions for 2012 and these are used for all EMEP4UK simulation years. Atmospheric CO_2 concentrations, which influence sulphate production and dry deposition of sulphur dioxide in this version of EMEP are fixed at 392 ppmv. Mixing ratios of methane are specified across the whole model domain at 1780 ppb for every year. O_3 boundary conditions at the edge of the European domain are based on climatological ozone-sonde data, modified monthly against climatological clean-air surface observations (Simpson et al. 2012). Hence, the same present-day O_3 boundary conditions for the outer European domain are used for each year. This excludes the influence



of climate-driven concentration changes outside the European domain on European air quality but allows us to isolate the signature of climate change over Europe alone.

2.3 Coupled Regional and Urban-scale modelling

The Atmospheric Dispersion Modelling System (ADMS) Urban model version 3.4.6 is used in this study. ADMS-Urban is a
205 quasi-Gaussian model that simulates the dispersion of emissions based on meteorological stability, which is influenced by urban land use and building morphology (Carruthers et al. 1994; Stocker et al. 2012; Hood et al. 2018). The model uses meteorological profiles of wind speed and direction, among other parameters, to define atmospheric conditions. Emissions from industrial, domestic and road traffic sources are included, either explicitly with detailed time-varying profiles e.g., for major road and industrial sources, or as 1 km grid-averaged emissions. A street canyon module modifies the dispersion of
210 emissions from all roads in the modelling domain with adjacent buildings, while an urban canopy module calculates modified wind speed and turbulence flow profiles to represent larger-scale urban conditions. ADMS-Urban uses a semi-empirical NO_x photolytic chemistry module (Venkatram et al., 1994), which accounts for fast, near-road oxidation of NO by O₃ to form NO₂ (Smith et al., 2017) and a simplified sulphate chemistry scheme for conversion of SO₂ to PM_{2.5}. The NO_x chemistry scheme performance has been compared with the detailed Master Chemical Mechanism over London by Hood et
215 al. (2018). This highlighted reasonable agreement (within 20-40%) except during summer air pollution episodes (Malkin et al. 2016). Further details of the ADMS-Urban model set-up can be found in Hood et al. (2018).

Emissions for all sources other than road traffic are from the London Atmospheric Emissions Inventory 2010 (GLA, 2013), projected from the LAEI base year 2010 to the modelled year 2012. Time-varying profiles are applied. Road traffic emissions were calculated using activity data from the LAEI with adjustments to NO_x, NO₂ and PM_{2.5} emissions factors to
220 improve consistency with real-world emissions measurements as described in Hood et al. (2018). The ADMS-Urban outputs for this study are for specified receptor locations corresponding to 56 reference air quality monitoring sites from the Automatic Urban and Rural Network (AURN) and from the London Air Quality Network (LAQN) (Hood et al. 2018).

The coupled WRF-EMEP4UK-ADMS-Urban regional to urban model system is used to simulate continental and urban street-scale air pollution and relevant metrics. Consistent anthropogenic emissions for the year 2012 are used in WRF-
225 EMEP4UK and ADMS-Urban. Hourly meteorological and chemical boundary concentrations from WRF-EMEP4UK grid-cells are used as input to ADMS-Urban through one-way coupling. This ensures that the long-range transport and chemical environment is adequately represented in terms of physical and chemical processes at all relevant time and spatial scales, from regional to street scale. The coupled system and the standard ADMS-Urban model configuration for 2012 is extensively evaluated in Hood et al. (2018).

230 2.4 Present-day and future model experiments

Present-day and future experiments were performed using the regional and urban coupled models to quantify changes in atmospheric composition due to climate change under RCP 8.5 at the regional scale over Europe and the UK and at urban



scale over London. Air quality metrics were calculated to evaluate the implications for attaining World Health Organisation (WHO) air quality guidelines and interim targets (WHO 2021).

235 Coupled model simulations were performed for two 10-year time periods: present-day (1996-2005) and future (2090-2099) following RCP8.5 using HadGEM2-ES climate outputs based on historical and RCP8.5 (Lamarque et al. 2010; Meinshausen et al. 2011) future simulations from CMIP5. The difference between these two periods results in a large global mean near-surface temperature change of 4.7°C (Met Office Hadley Centre, 2012). Anthropogenic emissions representative of the year 2012 (Sect. 2.3) are used for all 10-year present-day and future simulations in order to isolate the impacts of climate change 240 alone on atmospheric composition. The model set-up enables quantification of the coupled EMEP4UK and ADMS-Urban responses to climate change due to the combined effects of changes in atmospheric chemistry and physics processes, climate-sensitive emissions, deposition and transport (Sect. 1).

3. Regional-scale Climate Change impacts over Europe

245 This section examines the impacts of climate change on annual and season mean distributions of O₃, PM_{2.5} (both total and individual components) and their precursors, assuming no change in anthropogenic emissions.

3.1 Annual and Seasonal mean changes

Annual mean near-surface temperatures increase by more than 4°C across Europe and up to 8°C in northern Scandinavia and Alpine regions under RCP 8.5 in the 2090s (2090-2099) compared to 2000s (1996-2005; Fig. 1d). HadGEM2-ES suggests little change in temperature over the North Atlantic, a common feature of other CMIP models, and this has been attributed to 250 a reduction in the meridional overturning in this Atlantic Ocean region (e.g., Park and Yeh 2024).

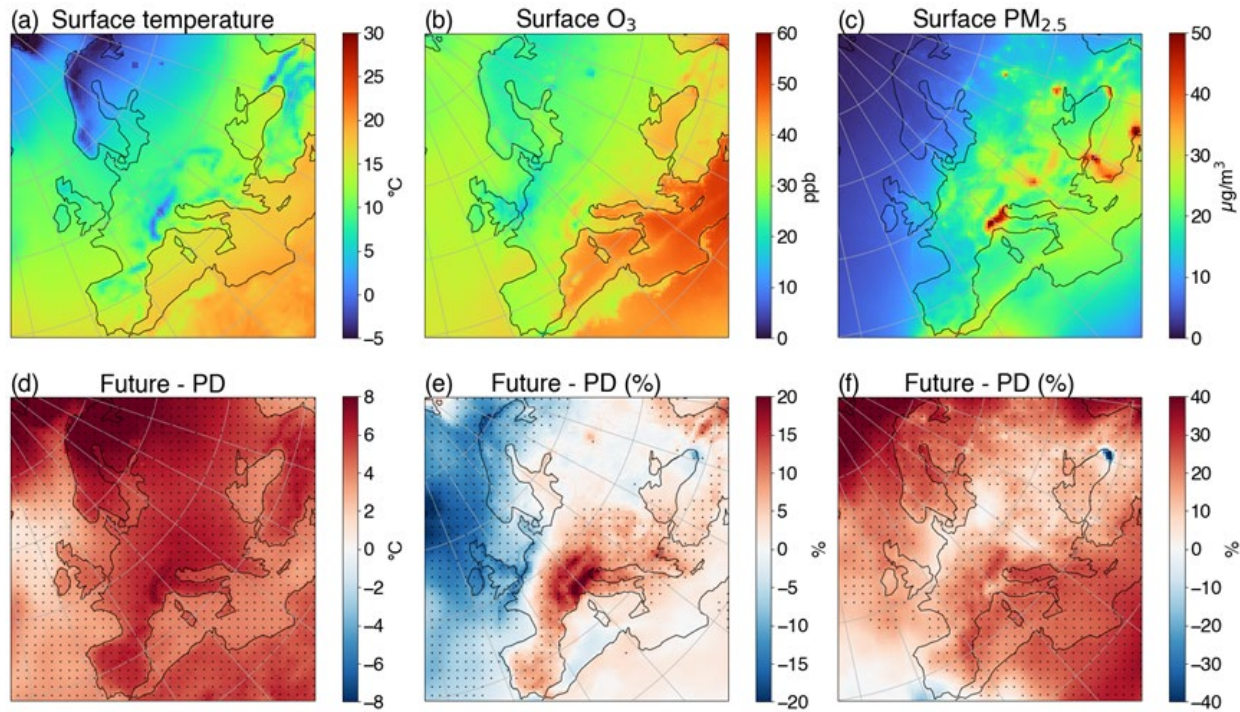


Figure 1: Annual mean distributions of a) temperature (2 metres) (°C), b) surface O₃ (ppbv) c) surface PM_{2.5} (µg m⁻³) for present-day (1996-2005) and the differences between future (2090-2099) – present day (1996-2005) in d) temperature (2 metres), e) surface O₃ f) surface PM_{2.5} (same units) simulated by WRF EMEP4UK (50km x 50km European domain). Statistically significant changes between the 10-year present-day and future periods are depicted as dots (student t-Test with a p value < 0.05).

255

260

265

270

Present day annual-mean surface O₃ mixing ratios averaged over the period 1996-2005 show a North-South gradient, with values greater than 30 ppbv in southern parts of Europe (higher over the Mediterranean and the Alps) and lower values ~20 ppbv in northern Europe (Fig. 1b). The annual mean O₃ response to climate change shows a strong regional contrast, as noted in previous studies for summer O₃ (e.g. Colette et al. 2015; Schnell et al. 2016; Sect. 1), with statistically significant increases of up to 20% over southern and central Europe (centred on the Alps) and decreases of up to 15% over northern Europe (Fig. 1e). Present-day annual-mean PM_{2.5} concentrations are typically between 10-20 µg m⁻³ but show hotspot locations e.g., northern Italy ~50 µg m⁻³ (Fig. 1c). Annual mean PM_{2.5} concentrations are elevated over most of Europe (up to 30%; typically between 5-10 µg m⁻³) under RCP8.5 (Fig. 1f); these values are similar in sign but higher than reported from global models following RCP8.5 and SSP3-7.0 pathways in previous studies (Silva et al. 2017; Turnock et al. 2022; Gomez et al. 2023).

To understand the drivers of these changes, winter and summer mean changes in O₃, PM_{2.5} and key precursor species are shown in Fig. 2. The response of surface O₃ to climate change exhibits a strong contrast between winter and summer. In winter, surface O₃ decreases significantly over a substantial part of continental Europe (2-8 ppbv; Fig. 2a), whilst in summer substantive O₃ increases are evident across nearly all of continental Europe (5-10 ppbv; Fig. 2f); with small decreases (that are statistically significant at the 95 % confidence interval) over Nordic regions and the UK, consistent with the findings of



Colette et al. (2015). In this warmer climate, increased water vapor concentrations reduce background O_3 levels, explaining reductions across the Atlantic in both seasons, and may largely drive the O_3 decreases across northern Europe in winter. The response of surface $PM_{2.5}$ to climate change is far more muted in winter compared to summer which shows significant increases of up to $15 \mu\text{g m}^{-3}$ in parts of Southern Europe, the Mediterranean and Northern Africa (Fig. 2b, g).

275

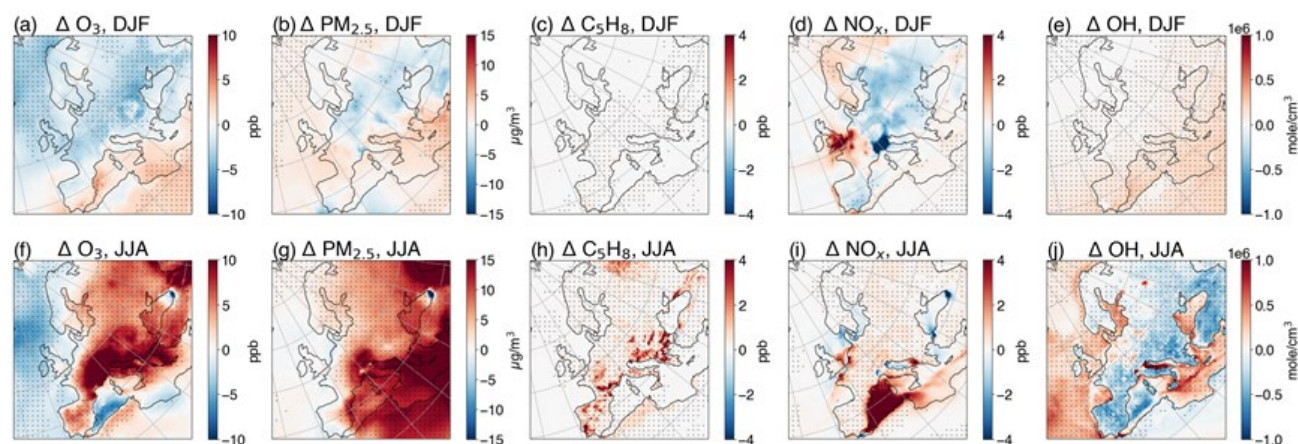


Figure 2: Top panels show winter mean distributions of surface changes in a) O_3 (ppbv), b) $PM_{2.5}$ ($\mu\text{g m}^{-3}$) c) isoprene (ppbv) d) NO_x (ppbv), and e) $OH \times 10^6$ (molecule cm^{-3}), under future conditions (2090-2099) compared to the present day (1996-2005). Lower panels (f-j) show the corresponding summertime changes. Statistically significant changes between the 10-year periods are indicated with dots (student t-Test with p value < 0.05).

280

Whilst anthropogenic emissions remain unaltered, biogenic isoprene emissions respond to elevated temperatures. Annual-mean isoprene emissions double across Europe with a tripling in hotspot locations (as in Fig. 2h), resulting in isoprene mixing ratios significantly elevated by up to 4 ppb in summer in parts of southern Europe, with much smaller changes in winter (Fig. 2c, h). These elevated isoprene levels are the main driver of higher O_3 and $PM_{2.5}$ in summer across continental Europe. Consistent with changes in isoprene, α -Pinene concentrations also strongly increase with temperature in both winter and summer throughout Europe (except in northern Scandinavia)(not shown).

285

Dry deposition of O_3 is also altered significantly by climate change. Across almost all of Europe, future wintertime deposition velocities that are up to 0.1 cm s^{-1} larger contribute to lower surface O_3 mixing ratios in winter, whilst deposition velocities up to 0.1 cm s^{-1} ($\sim 15\%$) smaller support higher surface O_3 in summer (Fig. 3a, d). Climate change simulations under the SRES A2 scenario found reductions in O_3 deposition velocities in summer of up to 40% over southern Europe between 1961–1990 and 2071–2100, leading to increases in summer mean O_3 of up to 6 ppbv (Andersson and Engardt, 2010). Vieno et al. (2010) also noted severely restricted O_3 dry deposition during the 2003 heatwave in the UK.

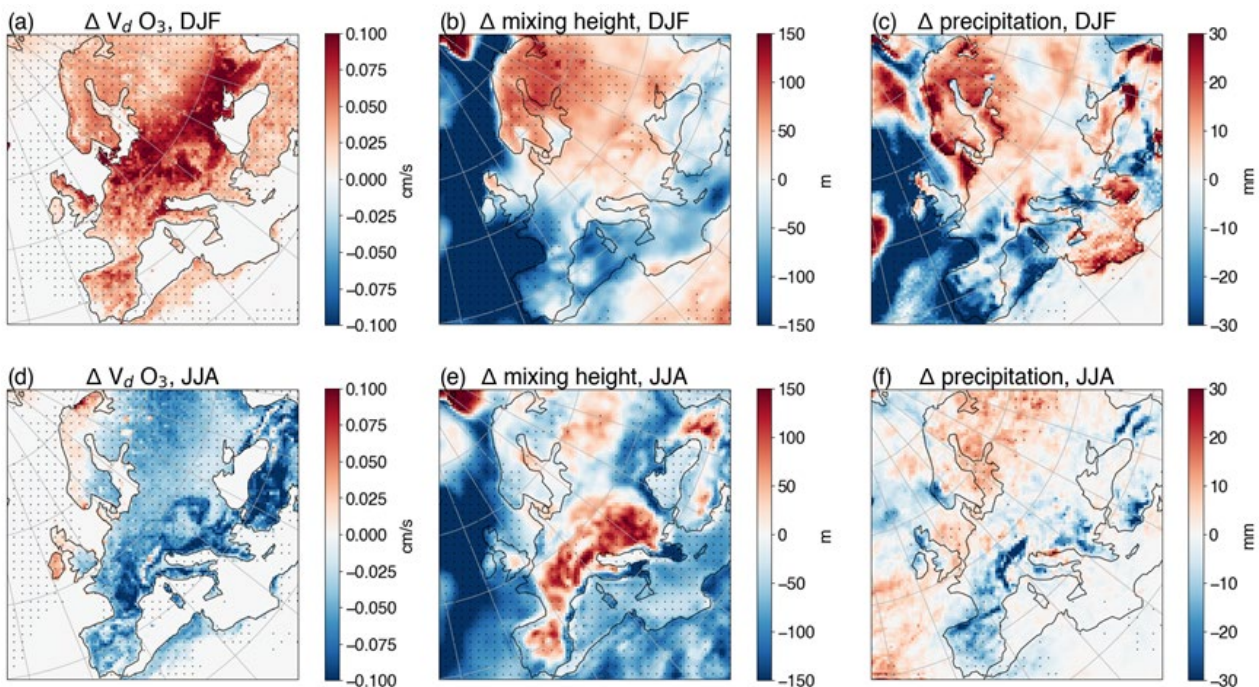


Figure 3. Top panels show wintertime changes in (a) O_3 deposition velocities (cm s^{-1}), (b) mixing layer height (m) and (c) precipitation (mm) in future (2090-2099) compared to the present day (1996-2005). Bottom panels (d-f) show the corresponding summertime changes. Statistically significant changes between the 10-year periods are indicated with dots (student t-Test with p value < 0.05).

Changes in oxidants were also examined. Hydroxyl radical (OH) concentrations generally increase slightly in winter but decrease more prominently in summer over most of Europe and the Mediterranean by up to 0.75×10^6 molecules cm^{-3} , with small OH increases for the UK and Benelux regions (Fig. 2e, j). These changes are statistically significant at the 95 % confidence interval. Most oceanic regions show summer increases reflecting greater OH production associated with higher humidity and O_3 destruction. HO_2 and RO_2 radical species also change slightly in winter, but exhibit an opposing response to that of OH, that is similar or greater in magnitude. There are many formation and loss processes affecting oxidant levels that may be influenced by climate change. In summer, the primary influence on OH changes across continental Europe is likely to be higher abundances of biogenic VOCs, whose oxidation acts as a OH sink that enhances HO_2 and RO_2 levels. In winter, the small uniform OH increases may be a consequence of greater OH formation as a result of higher O_3 destruction due to humidities.

Annual-mean soil NO_x emissions increase under this large climate signal by up to a factor of two (not shown) across almost all of Europe, potentially influencing land summer NO_x concentrations (Fig. 2i), but unlike isoprene, this natural soil emission source is minor compared to current anthropogenic NO_x emissions. In response to climate change, surface NO_x mixing ratios show distinct patterns of change over Europe in winter that are most prominent over major source regions. NO_x increases strongly over the UK, Benelux region and northern France (~ 4 ppbv) but generally decrease elsewhere, most



notably over northern Italy (4 ppbv; Fig. 2d,i), although these changes are not found to be statistically significant. In contrast, in summer there are small but significant NO_x increases over Europe, with large increases apparent in a few emission 315 regions, and notably over the Mediterranean coincident with OH reductions. The most prominent changes in NO_x mixing ratios over land are more localised than the O_3 and $\text{PM}_{2.5}$ responses reflecting the shorter atmospheric lifetime of NO_x . In winter, the areas of largest change are coincident with strong NO_x emission source locations. Winter NO_x increases in 320 northern European source regions are consistent with the findings of previous studies that highlight the reduced role of peroxyacetyl nitrate (PAN) with warmer temperatures. Using a global model, Doherty et al. (2013) found a widespread increase in annual mean surface O_3 of up to 1 ppbv over Europe under a global warming signal of 3°C, as a result of higher NO_x concentrations over source regions due to greater PAN decomposition. However, winter NO_x decreases in southern 325 Europe suggests photochemistry or mixing effects may be more important. In summer, reduced formation of PAN and OH decreases may increase NO_x lifetimes and promote higher NO_x over sources regions in Europe and the Mediterranean. Higher latitude increases in surface NO_x suggest titration of O_3 by NO in winter, that leads to reduced O_3 mixing ratios, as 330 photochemistry is less active to replenish O_3 in northern Europe. (Fig 2a, e). In southern Europe, reduced surface NO_x in winter is coincident with lower O_3 mixing ratios. To investigate the O_3 chemical environment the changes in NO_x/VOC concentration ratios are depicted in Fig. S1. There is a strong contrast between northern and southern Europe in winter with the highest ratios, indicating most VOC-limited conditions, over Benelux and the UK. In summer marine regions with heavy 335 shipping in the North Sea, English Channel/North Atlantic and the northern Mediterranean display the highest NO_x/VOC ratios. NO_x/VOC ratios increase in winter in northern Europe due to higher NO_x suggesting climate change would lead a more VOC-limited regime in future here, and decrease elsewhere suggesting more widespread NO_x -limited regimes (Fig. 1c). Conversely, in summer NO_x/VOC ratios decrease over continental Europe because of higher biogenic VOC levels due to 340 climate change, implying a more NO_x -limited regime, but increase over the Mediterranean due to higher NO_x (Fig. S1f). The different seasonal and latitudinal responses in the NO_x/VOC ratio highlight the challenge for designing future O_3 mitigation 345 strategies across Europe when considering the impacts of climate change. Overall, it is clear that climate-driven changes in isoprene emissions, O_3 dry deposition and chemistry have impacts on oxidant levels and surface O_3 right across Europe, as reported in previous studies.

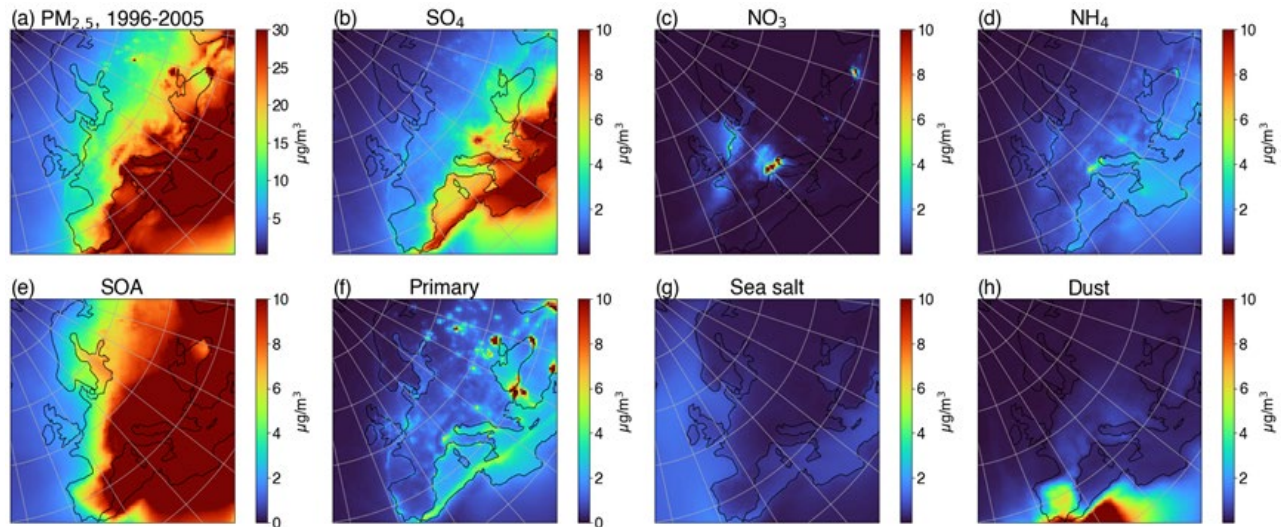
Climate change may also influence local mixing and transport patterns. Mean mixing heights over the 10-year present-day and future periods show distinct patterns of change over Europe. In winter, mixing heights decrease significantly over 350 western Europe and ocean regions and increase over central, eastern and northern Europe by up to ~100 m (Fig. 3b). In summer a strong land-ocean contrast is evident, with significant increases over continental Europe (up to 150 m) and decreases over oceans (Fig. 3e). In winter, over central Europe, the spatial pattern of surface O_3 and NO_x decreases resembles that of mixing height increases, suggesting that changes in mixing height may influence their responses to climate change. In summer, O_3 and $\text{PM}_{2.5}$ responses do not appear to be impacted by changes in boundary layer mixing height. 355 Precipitation in winter exhibits a similar east-west contrast, with increases in central and northern Europe and decreases in western Europe that are statistically significant (~10 mm and up to 30 mm; Fig 3c). Summer precipitation changes are mixed



across Europe with increases in eastern areas and larger reductions over mountainous regions (Alps/Pyrenees) (Fig. 3f). These precipitation changes may also influence PM_{2.5} concentrations e.g., increases over the Alps in summer (Fig 2g). Several previous global model studies have suggested that reduced large-scale precipitation over northern hemisphere 350 midlatitudes land regions under climate change especially in summer may lead to increases in surface PM_{2.5} due to less wet deposition (Allen et al. 2016; Banks et al. 2022).

3.2 PM composition changes

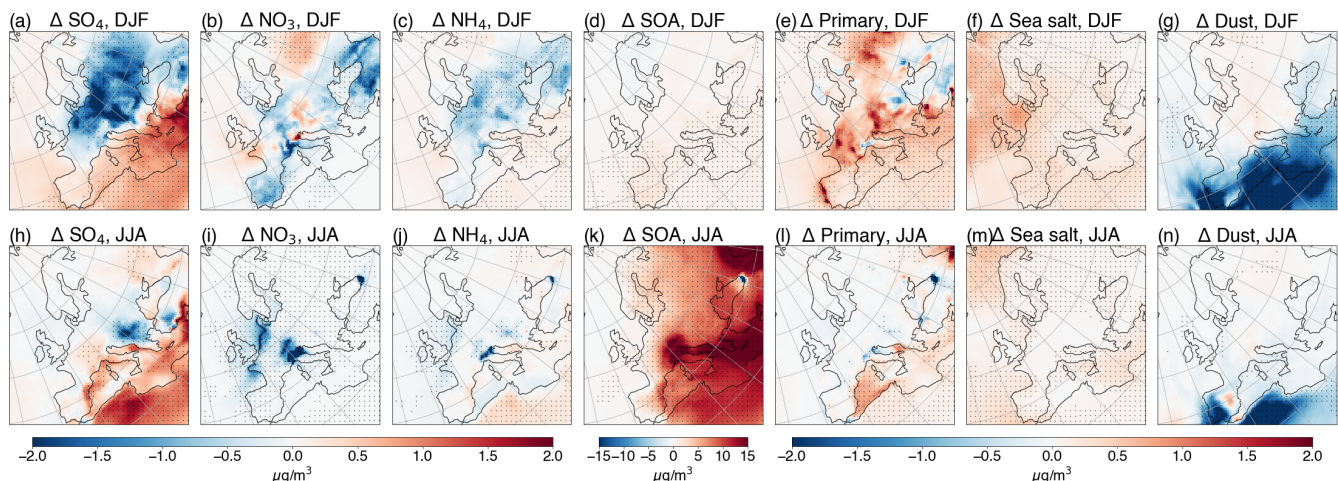
In the absence of anthropogenic emission changes, climate change impacts PM_{2.5} through changes in natural aerosols and/or aerosol precursor emissions, oxidising capacity and secondary aerosol formation pathways, and/or aerosol sink processes. In 355 this section we assess how the composition of annual and seasonal mean PM_{2.5} may change in the future, and the key driving processes. The present-day (1996-2005) spatial distribution of annual-mean PM_{2.5} components in Fig. 4 highlights that the inorganic contribution to PM_{2.5} is dominated by sulphate from energy generation in south east Europe and shipping in the Mediterranean, as well as nitrate (and to a lesser extent ammonium) in the Alps/Po valley region. Primary black and organic 360 carbon emission hotspots are responsible for a strong urban/anthropogenic fingerprint and a large natural Saharan dust component is also evident in overall PM_{2.5} levels, particularly over south-west Europe. A substantial widespread secondary organic source of PM_{2.5} is evident almost everywhere. In winter, the abundances of sulphate, nitrate and primary PM_{2.5} are larger over land, whilst in summer sulphate is higher over the Mediterranean and SOA levels are substantially higher (exceeding 10 $\mu\text{g m}^{-3}$) over all of continental Europe and the Mediterranean (not shown).



365 **Figure 4:** present-day (1996-2005) spatial distributions of annual mean a) PM_{2.5} and its secondary components: b) sulphate (SO₄), c) nitrate (NO₃), d) ammonium (NH₄), e) secondary organic aerosol (SOA); and primary components: f) primary organic matter and elemental carbon, g) sea salt and h) desert dust aerosol; all in $\mu\text{g m}^{-3}$.



370 The seasonal changes in these $\text{PM}_{2.5}$ components in the 2090s compared with 2000s are shown in Fig. 5. Numerous climate
sensitive processes influence the concentrations of inorganic aerosol in the atmosphere. Of the inorganic components of
 $\text{PM}_{2.5}$, sulphate displays the largest response to climate change under RCP8.5. Sulphate aerosols exhibit a large and
statistically significant wintertime decrease ($> 2 \mu\text{g m}^{-3}$) over central Europe and an increase over ocean regions (Fig. 5a). A
smaller significant summertime decrease in sulphate occurs over the Balkan regions with more widespread increases
375 (notably in the Mediterranean) or no change elsewhere (Fig. 5h).



380 **Figure 5: Top panels show changes in spatial distribution of $\text{PM}_{2.5}$ components in winter due to climate change: a) sulphate (SO_4), b) nitrate (NO_3), c) ammonium (NH_4), d) SOA e) primary organic matter and elemental carbon, f) sea salt and g) desert dust aerosol, all in $\mu\text{g m}^{-3}$ in future (2090-2099) compared with present day (1996-2005) conditions. The lower panels (h-n) show the
corresponding changes in summertime. Statistically significant changes between the 10-year periods are indicated with dots
(student t-Test with p value < 0.05).**

A key driver of winter changes in sulphate levels in the 2090s is changes in its deposition. Both wet deposition of sulphur
dioxide (SO_2) and dry deposition of SO_x ($\text{SO}_2 + \text{SO}_4$) and increase prominently in winter over central Europe (Fig. S2a, b),
385 whilst SO_2 concentrations decrease significantly, and hence there is less sulphate formation. Greater washout of SO_2 seems
likely associated with higher precipitation over this region (Fig. 3c). In addition, the winter increase in mixing height may
reduce sulphate aerosol levels at the surface (cf. similar spatial features Fig. 3b, Fig. 5a). Similar wet deposition (Racherla
and Adams 2006) and precipitation responses over continental land regions have been reported in previous studies (e.g.,
Allen et al. 2016). Other studies have noted winter sulphate decreases in Northern Hemisphere industrialised regions
390 associated with oxidant limitation (Berglen et al. 2004; Shindell et al. 2009). As noted in section 3.1, OH increases slightly
in winter in the future (Fig. 2e), suggesting oxidant limitation does not worsen in the future. However, O_3 is also important
for in-cloud oxidation of SO_2 to SO_4 and lower O_3 concentrations in winter suggest this could be important in limiting SO_4
formation. In summer, the decreases in wet and dry deposition of SO_2 and SO_x respectively (Fig. S2e, f) over the Balkans



395 coincide with lower sulphate concentrations (Fig. 5h), suggesting that deposition is not the main driver of this sulphate response. Under a warmer climate, an increase in sulphate loading could be expected as the oxidation of SO_2 to sulphate is faster at higher temperatures. However, as both SO_2 and OH (Fig. 2j) decrease in summer in this region, a reduced level of reactants may explain the sulphate decreases. Over the Mediterranean region, a combination of processes, such as faster oxidation with higher OH in eastern seas, seems likely to cause elevated sulphate aerosol concentrations in both seasons.

400 The response of nitrate aerosol to climate change in winter is mixed across Europe but with more widespread decreases ($0\text{--}1 \mu\text{g m}^{-3}$) than increases; in summer, nitrate decreases in some hotspot emissions source locations (Fig. 5 b, i). In the future, dry deposition of oxidised nitrogen increases over the European continent in winter; with a more mixed response in summer (Fig. S2c, g). Wet deposition of nitric acid (HNO_3) is similarly influenced by climate-driven changes in precipitation in winter but only increases slightly over central and northern Europe and decreases elsewhere (Fig. S2d). Hence winter nitrate decreases across Europe seem influenced mainly by dry deposition increases than wet deposition responses. The response of 405 this semi-volatile species to climate change may also be driven by enhanced partitioning into the gas phase with higher temperatures in both winter and summer reducing nitrate aerosol concentrations, as noted in other studies (Dawson et al. 2007, Pye et al. 2009). Ammonium concentrations (up to $1 \mu\text{g m}^{-3}$) and wet deposition of reduced nitrogen also decrease mostly strongly in winter over the European continent (Fig. 5j) reflecting concomitant reductions in sulphate and nitrate aerosol loadings.

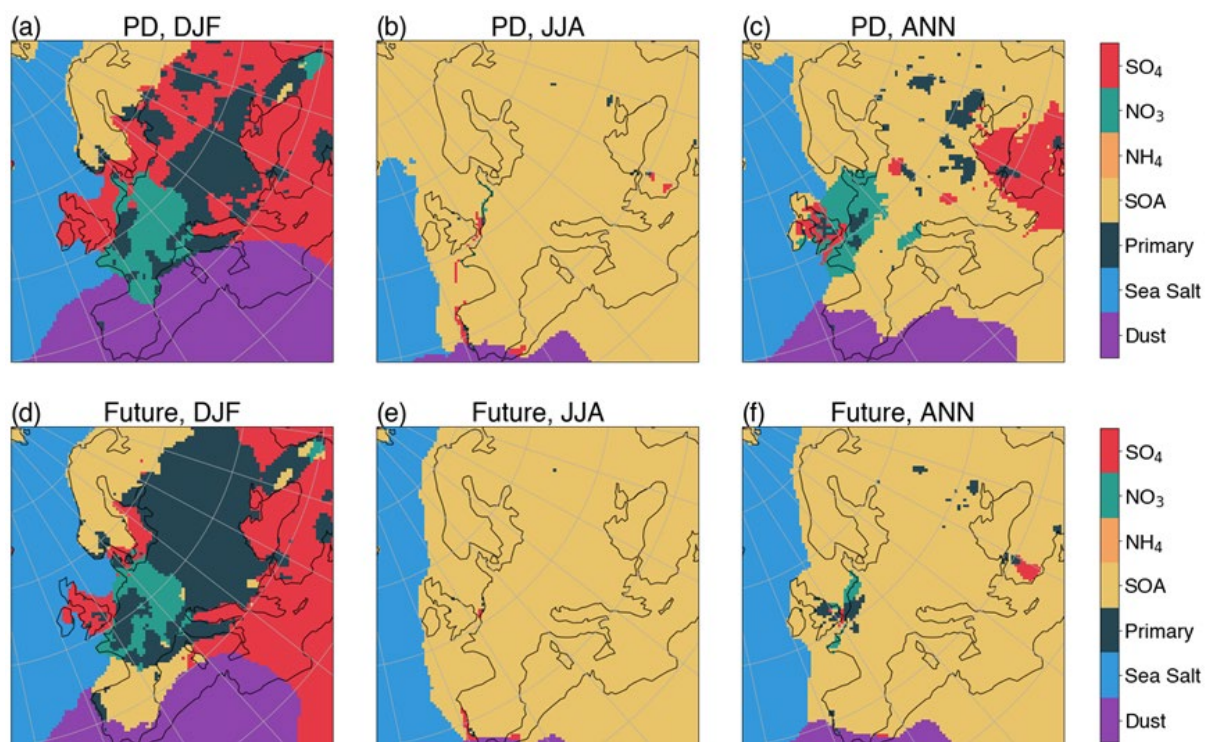
410 SOA shows by far the largest and most widespread summertime increase across Europe of all the $\text{PM}_{2.5}$ components ($>5 \mu\text{g m}^{-3}$) in the 2090s driven by the response of its natural isoprene and monoterpene precursor sources to climate change (Fig. 5k). Increases are also found in winter across continental Europe that are largest over western Europe (up to $2 \mu\text{g m}^{-3}$). Primary $\text{PM}_{2.5}$ sources are also influenced by climate change. There are notable wintertime future increases in primary fine 415 organic matter and fine elemental carbon concentrations in source regions which can be related to reductions in precipitation over certain regions (cf. Fig. 3c, Fig. 5e), but little change in summer.

Sea salt and dust, that contribute a small fraction of their mass to $\text{PM}_{2.5}$, are sensitive to changes in wind speed and transport patterns. Sea salt aerosol loadings increase slightly in the future (up to $0.5 \mu\text{g m}^{-3}$ across Europe) whilst desert dust from the 420 Sahara strongly decreases (by more than $2 \mu\text{g m}^{-3}$) in both seasons in the future (Fig. 5f-g,m-n). Both components primarily affect oceanic and maritime regions. These modified distributions in sea-salt and dust aerosols can be explained by changes in wind speed under RCP8.5 in the 2090s. Wind speeds generally increase by up to 1 m s^{-1} in the Atlantic in both seasons and by $>2 \text{ m s}^{-1}$ polewards of 60°N in winter, aiding sea-salt aerosol formation; whilst wind speeds are reduced over the Mediterranean in both seasons, hindering Saharan dust transport (by up to 1 m s^{-1} ; Fig. S3c, f). Similar responses were seen in a study by Turnock et al. (2022) under SSP3-7.0, which found enhanced sea salt aerosols in maritime parts of northern Europe and a reduction in fine dust aerosol across North Africa.

425 Primary organic matter and elemental carbon replaces sulphate (and to a lesser extend nitrate) to become the dominant component of wintertime $\text{PM}_{2.5}$ in the 2090s over central northern Europe (Fig. 6a, d). Across the Iberian Peninsula SOA replaces dust as the dominant winter $\text{PM}_{2.5}$ component (Fig. 6a, d). In summer, across all of continental Europe, SOA remains



the dominant $\text{PM}_{2.5}$ constituent in the future, whilst over certain oceanic locations (e.g., the Atlantic), the spatial dominance of Saharan dust decreases, and that of sea-salt increases in the future (Fig. 6b, e). Considering annual average $\text{PM}_{2.5}$, the most 430 evident changes are an increase in SOA as the dominant $\text{PM}_{2.5}$ component driven by the reduction in sulphate over Central Europe, the reduction in nitrate and sulphate over the North Sea and the reduction in Saharan dust over the Iberian Peninsula (Fig 6. c,f).



435 **Figure 6: Dominant components of $\text{PM}_{2.5}$ for present-day (1996-2005) for a) winter, b) summer, c) annual and for future (2090-2099) d) winter, e) summer, f) annual.**

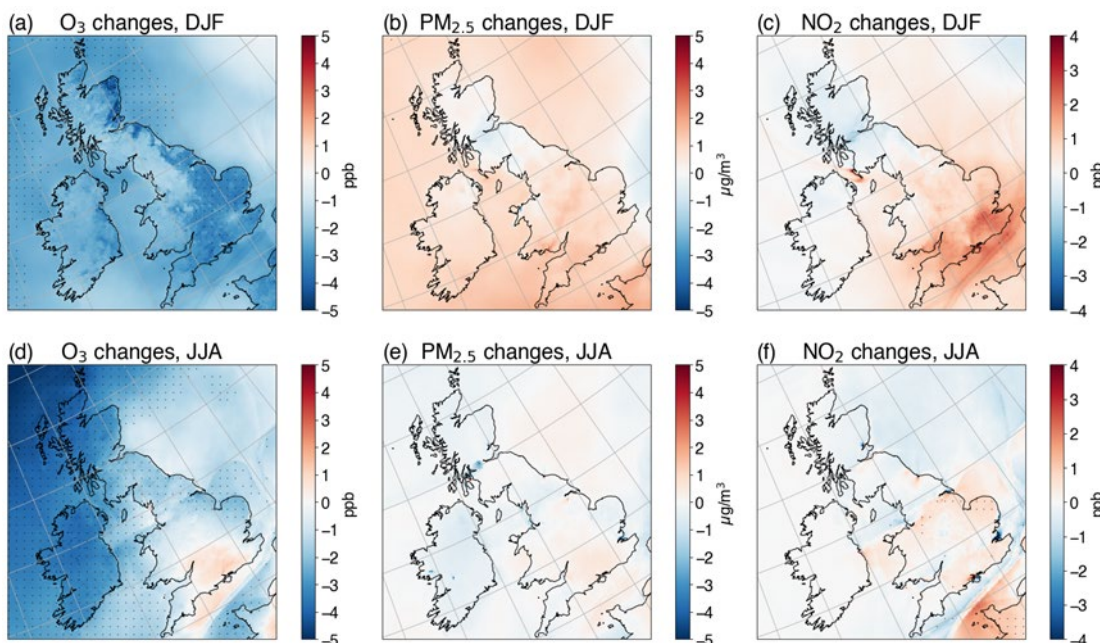
4. Climate change impacts over the UK and for London

This section examines simulated surface O₃ and NO₂ mixing ratios and $\text{PM}_{2.5}$ concentrations across the UK from the finer-scale regional EMEP4UK model at 5 km resolution. It then compares the seasonal cycles of these air pollutants between 440 EMEP4UK and the street-scale ADMS-Urban models and examines the diurnal variation of these species simulated by ADMS-Urban over London.



4.1 UK distributions

The finer-scale 5 km \times 5 km simulations show significant surface O₃ decreases across the UK of \sim 2-4 ppbv in winter in the 445 2090s compared to the 2000s with the largest decreases over eastern parts of the UK (Fig. 7a). Surface O₃ decreases of a similar magnitude occur in summer, except in the southern UK (including London) where there are O₃ increases of up to 1 ppbv in future (Fig. 7d). These patterns of change are similar to those seen in the European 50 km \times 50 km resolution model 450 domain in Fig. 2a, f; and largely due to background O₃ reductions. The magnitudes of winter and summer mean O₃ simulated over the UK at the finer resolution are about 2 ppbv (\sim 5%) higher than at the coarser resolution (Table A1). However, the changes between present-day and future climate at the two resolutions are only very slightly different (0.1/0.4 ppbv in DJF/JJA; Table A1). The magnitudes of the O₃ decreases are consistent with estimates of annual-average reductions from global models by Zanis et al. (2022), as reported in RS (2021), although Colette et al. (2015) report smaller summer O₃ decreases, likely due to the larger areal extent of their UK region that includes surrounding oceans.



455 **Figure 7:** Top panels show changes in winter due to climate change in a) surface O₃ mixing ratios (ppbv) b) surface PM_{2.5} concentrations ($\mu\text{g m}^{-3}$) c) surface NO₂ mixing ratios (ppbv) from EMEP4UK over the UK domain at 5 km \times 5 km resolution in future (2090-2099) compared with present-day (1996-2005). The lower panels (d-f) show the corresponding changes in summertime. Statistically significant changes between the 10-year periods are indicated with dots (student t-Test with p value < 0.05).

460 Surface PM_{2.5} concentrations simulated within the 5 km \times 5 km UK domain increase moderately in winter over much of the UK (\sim 1-2 $\mu\text{g m}^{-3}$) and show smaller (up to 1 $\mu\text{g m}^{-3}$) but mixed responses for summer with slight increases over southernmost UK in the future (Fig. 7 b, e). These patterns of changes again resemble those simulated over the UK with the



50 km × 50 km European domain (Fig 2c, d). However, these changes are not statistically significant at the 95 % confidence level. In both seasons, the magnitudes of PM_{2.5} simulated over the UK at the finer 5 km resolution are slightly lower (up to 465 2.1 µg m⁻³; ~10%) than at the coarser 50 km resolution, and the changes between present-day and future from the two resolutions for winter/summer differ marginally (~0.2 / 0.5 µg m⁻³; Table A1).

Surface NO₂ increases by ~2 ppbv in winter over the southern UK and the English Channel, but changes elsewhere in the UK are small (Fig. 7c, f). Smaller and mixed NO₂ responses are seen in summer. These differences are generally not statistically significant. Like the other two air pollutants, the patterns of NO₂ changes are very similar to those simulated at 470 the coarser resolution, with the magnitudes slightly lower (~1 ppbv; ~5%; Table A1) as found for PM_{2.5} changes at the coarser resolution. In summary, differences in horizontal resolutions employed by EMEP4UK model do not seem to influence the patterns, and only minorly influence the magnitudes, of changes in simulated concentrations of surface O₃, PM_{2.5} and NO₂ between present-day and future.

4.2 Regional- and Urban-scale Seasonal cycles for London

475 To explore the changes in key pollutants at an urban scale, concentrations at 56 receptor sites representing UK reference air quality measurement network locations across London are considered. Statistics based on these 56 locations for the ADMS-Urban model, are compared these with those from 10 model grid cells that span these locations from the EMEP4UK model simulations at 5 km × 5 km resolution. Surface O₃, PM_{2.5} and NO₂ distributions across London from both models are shown in Fig. 8, and median values are summarised in Table A2.

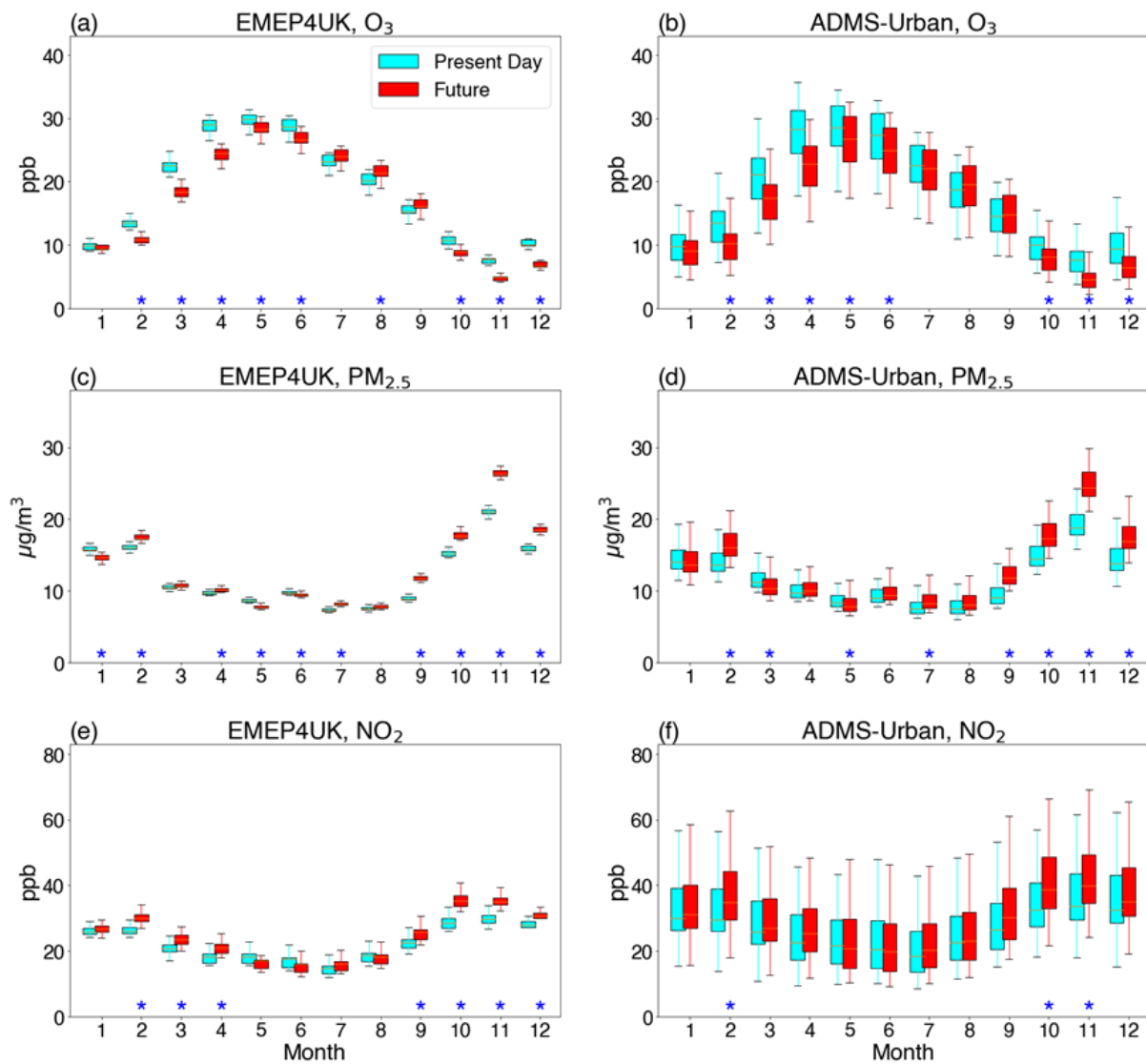


Figure 8: Seasonal cycles for present-day and future across London from EMEP4UK and ADMS-Urban for (a, b) surface O_3 , mixing ratios (ppbv) (c, d) $PM_{2.5}$ concentrations ($\mu g m^{-3}$) and (e, f) NO_2 mixing ratios (ppbv) respectively. Monthly mean values, calculated as averages over the respective 10-year periods for each of 10 EMEP4UK grid boxes and 56 ADMS-Urban locations, are used to produce spatial statistics represented by box (the interquartile range) and whisker plots. The blue star denotes months where surface distributions are significantly different between present-day and future according to a student t-Test with a p value < 0.05 .

The seasonal cycles of O_3 across London, from both the regional and urban street-scale models, have very similar amplitudes of ~ 20 ppbv; with the lowest median mixing ratios in winter of ~ 10 ppbv and highest in summer of ~ 30 ppbv (Fig. 8a, b). Differences in magnitudes of present-day values between the two models are relatively small (less than 1.5 ppbv; Table A2) and differences in future changes are also small (0.1-0.9 ppbv). Decreases in future O_3 mixing ratios (Sect 4.1) are largest in November and December, up to ~ 3 ppbv for both models. Surface O_3 over London has a springtime peak, and the amplitude



of this decreases significantly in future by up to 5 ppbv in April in both regional and urban-scale model simulations. This is in agreement with global model results for northern Europe by Schnell et al. (2016), who also noted changes in climate-sensitive BVOC precursor emissions could also impact seasonal cycles. In all months except January, July and September 495 (and August for ADMS-Urban) surface O₃ distributions simulated by the two models differ significantly between present-day and future.

Both models simulate an autumn/winter peak in the seasonal cycles of PM_{2.5} concentrations across London (median values ~20 µg m⁻³ in November and ~15 µg m⁻³ in December/January) that significantly increases in the future by as much as 5 µg m⁻³ in November (Fig. 8c, d; Table A2). In spring and summer, median surface PM_{2.5} concentrations (7-11 µg m⁻³) only 500 marginally change in the future. Comparing the two models, differences in both present-day values (up to 2 µg m⁻³ between November-February) and present-day and future changes (less than 1.1 µg m⁻³) are small. A previous street-scale modelling study for London using the ADMS-Urban model found different results because they neglected the processes affecting background O₃ (Athanassiadou et al. 2010).

NO₂ seasonal cycles also exhibit an autumn/winter peak (median value of ~30 ppbv in November) for both models with 505 median values between 15-26 ppbv in other seasons (Fig 8e, f; Table A2). Unlike for O₃ and PM_{2.5}, median monthly NO₂ values are consistently 3-5 ppbv higher (~15%) for the ADMS-Urban compared to the EMEP4UK model. This difference is likely to be due to the inclusion of near-road locations in the ADMS-Urban model, where NO₂ concentrations are strongly influenced by NO_x emissions from the nearest road. In the future, the largest increases in NO₂ mixing ratios, exceeding 4 ppbv for both models, occur in October, November and February and are statistically significant in both models.

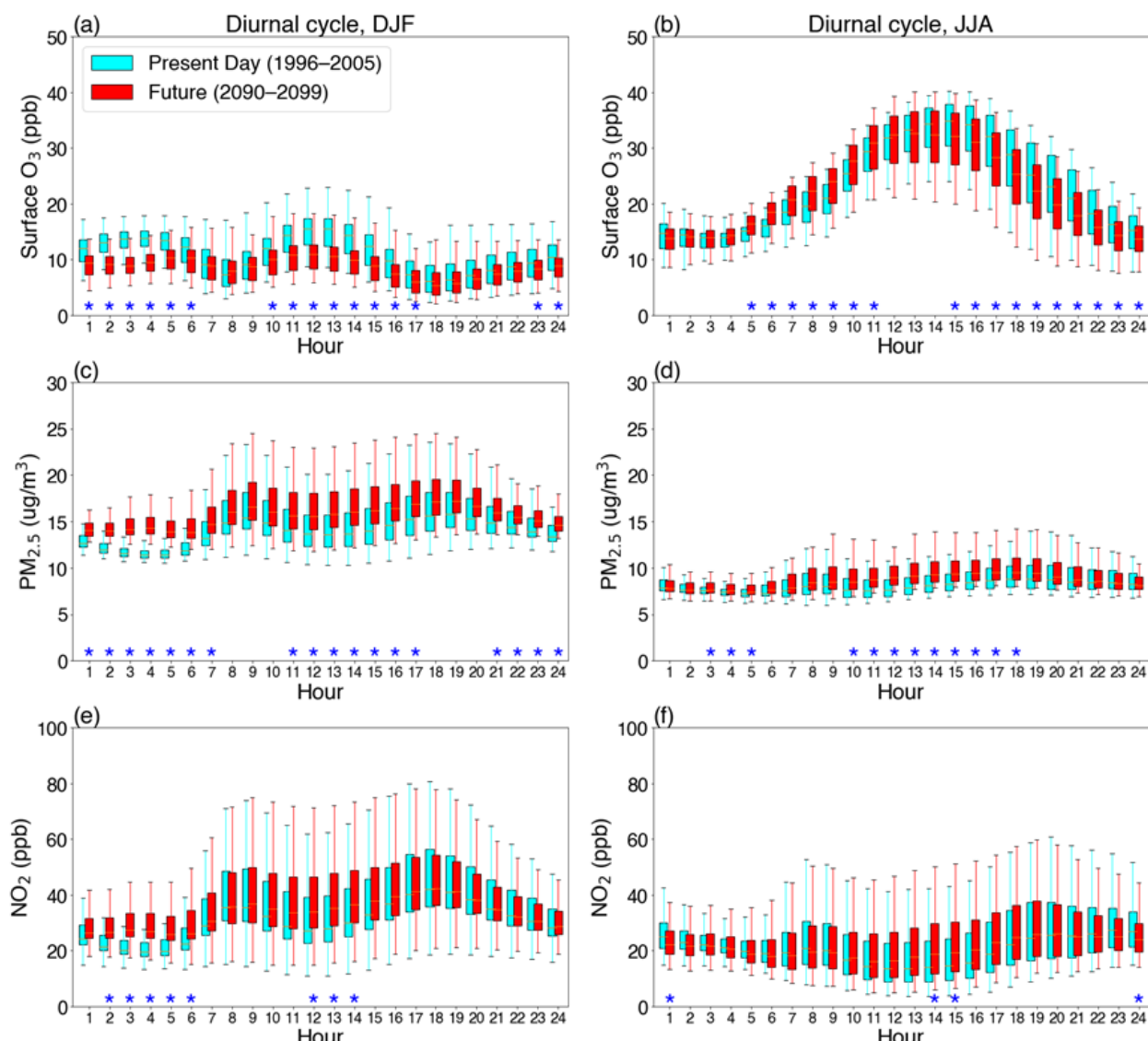
510 Overall, the magnitudes of the median monthly concentrations, and changes between present-day and future, are in good agreement between both models for all three air pollutants, although NO₂ values are higher. However, considerably larger spatial variability across the 56 locations is simulated by the urban street-scale (ADMS-Urban) model compared to the 10 fine-scale EMEP4UK regional model grid cells, and this is most prominent for NO₂. There are also fewer months with 515 significant differences between present-day and future distributions simulated for all three air pollutants simulated by the street-scale model as compared to the high-resolution regional model. The sensitivity of the street-scale model outputs to the number of sampling sites employed was examined by randomly sampling 10 of the 56 locations to produce distributions for London. Small changes between the results for 10 compared to 56 locations were found, adding confidence to the conclusion 520 that the street-scale simulation exhibits larger spatial variability in air pollutant concentrations due to its ability to explicitly represent road emissions sources as compared to the grid-box representation in the regional model that can lead to the dilution of emissions.

4.3 Urban-scale Diurnal cycles for London

The diurnal variation in surface O₃, PM_{2.5} and NO₂ concentrations simulated at 56 locations across London with the street-scale model is shown in Fig. 9. The diurnal cycle of surface O₃ mixing ratios is much more pronounced in summer than in winter due to longer daylight hours and higher temperatures increasing its photochemical formation, with daytime median



525 values exceeding 30 ppbv between 12 and 5 pm, and nighttime median values below 15 ppbv for present-day (Fig. 9b). In
 winter, the diurnal variation of surface O_3 is much flatter than in summer, with a slight afternoon peak (median value \sim 15
 ppbv at 12-1 pm) and evening to nighttime median levels of 6-13 ppbv (Fig. 9a). Across the 56 locations, the largest
 530 variability occurs in summer during afternoon to early evening hours (up to 10 ppbv for the interquartile range). A
 statistically significant decrease in winter surface O_3 in the future is apparent for early morning and afternoon hours. In
 summer, surface O_3 is significantly higher by up to 3 ppbv in the morning but significantly lower by up to 4 ppbv in the
 afternoon and evening in the future. This leads to a small shift in the diurnal cycle of summertime surface O_3 , with the peak
 occurring about one hour earlier, although the amplitude of the diurnal cycle remains very similar.





535 **Figure 9: Diurnal cycles for present-day and future from ADMS-Urban for (a, b) surface O₃ mixing ratios (ppbv) (c, d) PM_{2.5} concentrations (µg m⁻³) and (e, f) NO₂ mixing ratios (ppbv) for winter and summer respectively for London over 56 ADMS-Urban receptor locations sites. Data are hourly mean values averaged over the respective 10-year periods at each location to produce box (interquartile ranges) and whisker plots depicting the spatial variation across London. *Denotes months where surface distributions are significantly different between present-day and future according to a student t-Test with a p value < 0.05.**

540 For surface PM_{2.5} concentrations the diurnal variation in both seasons is relatively small with median concentrations between 11-16 µg m⁻³ in winter and ~8 µg m⁻³ in summer for present-day (Fig. 9c, d). The spatial variability across the 56 locations is largest for winter daytime hours (up to 4 µg m⁻³ for the interquartile range). Higher median wintertime levels (by up to 3 µg m⁻³) are evident at all times of day in the future, with statistically significant differences between present-day and future for most hours (Fig 9c). Additionally in winter, PM_{2.5} increases are considerably larger at night-time leading to reduced diurnal 545 variability in the future, with similar spatial variability. Summertime median levels are slightly higher during daytime with significant increases between 10 am and 6 pm of about 1 µg m⁻³ in the future.

The diurnal variation of NO₂ mixing ratios is similar to that of PM_{2.5} concentrations in winter, highlighting similar 550 anthropogenic emissions sources, but is more pronounced with median values around 20 ppbv between 2-5 am and increasing at 7 am and from 3 pm, reaching 42 ppb at 6 pm for present day (Fig 9e, f). Summer NO₂ mixing ratios additionally exhibit an early afternoon dip, likely related to the surface O₃ peak. In both seasons there is substantial spatial 555 variability, notably for daytime hours, across the 56 locations (up to 20 ppbv for the interquartile range) driven by differences in dispersion reflecting the differing proximities of the sites to road NO_x emissions sources (as noted in Hood et al. 2018). In the future, larger significant winter NO₂ increases (median values up to 7.6 ppbv) in the early morning lead to a flatter distribution, although significantly higher NO₂ also occurs in early afternoon (Fig 9e, f). In the summer, significant higher mid-afternoon NO₂ values also cause a flattened distribution in the future. The spatial variability for NO₂ across the 56 locations is similar for the two time periods. Fewer hours show statistical differences between present-day and future for NO₂, as compared to O₃ and PM_{2.5}, again due to the dominance of unchanged road emissions in NO₂ concentrations.

The broad changes in the diurnal cycles of surface O₃, PM_{2.5} and NO₂ concentrations are consistent with the changes in the 560 described in Sect 4.2 for the seasonal cycles of these air pollutants. Here, the effect of night-time/early morning changes in winter for the three air pollutants, and changes either side of peak levels for summer O₃ is additionally highlighted. Distributions of winter O₃, and PM_{2.5} and NO₂ in both seasons, flatten in the future.

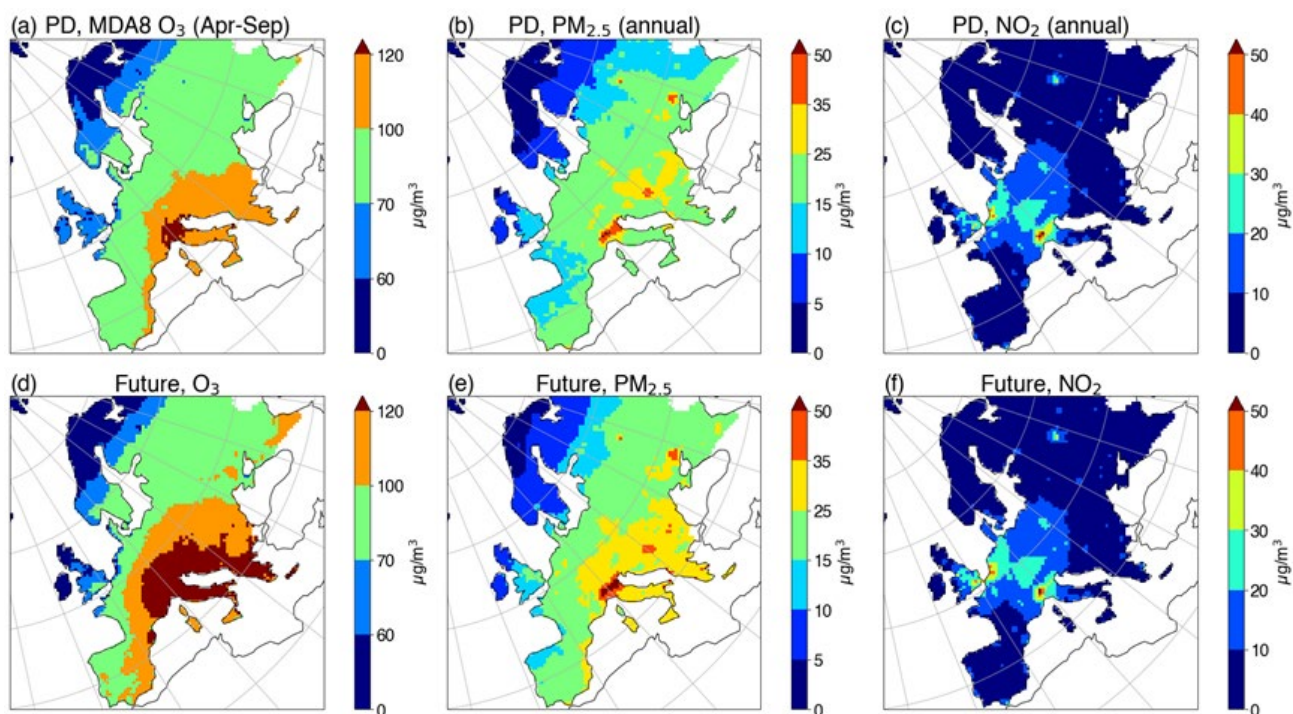
5. Implications for achieving long-term and short-term WHO guidelines.

These regional and street-scale results can be used to evaluate the likelihood of achieving the latest WHO air quality 565 guidelines (WHO 2021), under the RCP8.5 climate change signal as compared to present-day. These guidelines are based on two averaging periods to reflect the health effects associated with both acute and chronic exposures to air pollutants. For long-term exposure, peak season daily maximum 8-hour mean (MDA8) values are used for O₃ and annual mean concentrations for PM_{2.5} and NO₂. Short-term exposures utilise the 99th percentile value of MDA8 for O₃ and the 24-hour



mean for $\text{PM}_{2.5}$ and NO_2 . Interim target values towards achieving these more stringent air quality levels are also outlined. For present-day and future, long-term exposures are evaluated across Europe whilst short-term exposures are assessed for 570 London— as hourly outputs are only retained from the ADMS-Urban model simulations for this study. For peak season O_3 results over Europe (Fig. 10), MDA8 was estimated based on fitting a relationship between MDA8 and daily maximum and daily mean O_3 (the EMEP4UK outputs available) over London as follows:

$$\text{MDA8 } \text{O}_3 = \frac{2}{3} \times \text{daily maximum } \text{O}_3 + \frac{1}{3} \times \text{daily mean } \text{O}_3.$$



575 **Figure 10:** a) peak season (April to September) daily maximum 8-hour average (MDA8) O_3 and annual average b) $\text{PM}_{2.5}$ c) NO_2 concentrations for present-day (1996-2005) and d) MDA8 O_3 and annual average e) $\text{PM}_{2.5}$ and f) NO_2 concentrations for future (2090-2099) calculated from monthly mean values for each year averaged over the respective ten-year periods. Scales depict interim target values and the air quality guidelines for each of these air pollutants. For MDA8 interim targets are 100 and $70 \mu\text{g m}^{-3}$ and the air quality guideline (AQG) is $60 \mu\text{g m}^{-3}$. For $\text{PM}_{2.5}$ interim targets are 35, 25, 15, $10 \mu\text{g m}^{-3}$ and the AQG is $5 \mu\text{g m}^{-3}$. For NO_2 interim targets are 40, 30, $20 \mu\text{g m}^{-3}$ and the AQG is $10 \mu\text{g m}^{-3}$ (see WHO, 2021).

The immediate and future challenges for Europe, and especially southern Europe, to attain these interim targets and guidelines for long-term O_3 exposure based on the regional model simulations are clear. The peak season first interim target is largely met except over southern Europe but the second interim target is only achieved in northernmost Europe, whilst the 585 air quality guideline is only met in northern Scandinavia and a few locations in the UK and Benelux region (Fig. 10a). In the future, fewer areas of continental Europe meet the first interim target and smaller parts of northern Europe meet the second interim target (Fig. 10d). As for present-day, the air quality guideline value of $60 \mu\text{g m}^{-3}$ is only met in parts of northernmost Europe in the future. However, the areal extent of attainment of this air quality guideline value expands and extends to larger



parts of the UK, due to background surface O₃ decreases within parts of this region. Examining extreme O₃ episodes (87th percentile), Schnell et al (2016) found qualitatively similar results with higher O₃ levels, implying less attainment of these air quality guidelines in the future under RCP8.5 for southern Europe for 3 out of 4 global models; as well as small reductions in percentile values, aiding attainment of air quality guidelines, for northern Europe.

For PM_{2.5}, for present-day, the first interim target is met across Europe except in a few hotspot regions, and the second interim target is also largely achieved (Fig. 1c, Fig. 10b). In contrast, much of continental Europe does not meet the third interim target for present-day in these simulations. Very limited parts of Scandinavia and the UK meet the fourth interim target and even fewer locations achieve the 5 $\mu\text{g m}^{-3}$ air quality guideline (Fig. 10b). In the future, the first interim target remains largely achieved, fewer areas in southern and Central Europe achieve the second interim target, the third interim target is exceeded across almost all of continental Europe, less of Scandinavia achieves the 4th interim target and only northernmost Scandinavia meets the air quality guideline (Fig. 10e).

For NO₂ for present-day and future, the first and second interim targets are achieved everywhere except in a few hotspot locations such as in the Po valley and the Netherlands (Fig. 10c). The third interim target is also largely met except in parts of western and central Europe and the southern UK. Much of western, easternmost and northern Europe achieve the NO₂ air quality guideline, but western-central Europe does not. Differences in attainment of this air quality guideline between present-day and future are small (Fig. 10f) due to large anthropogenic contribution to NO₂ levels.

Overall, the current WHO air quality guidelines for long-term exposure to peak season MDA8 O₃ and annual average PM_{2.5} are challenging to achieve across most of Europe in the present-day; based on the 2012 anthropogenic emission dataset employed in this study. They become increasingly difficult to achieve in the future under the effects of a changing climate except in a few northern locations, meaning that future mitigation of anthropogenic emissions will need to go further to achieve benefits to human health. As noted above, these findings are sensitive to anthropogenic emissions levels. For NO₂, under these 2012 anthropogenic emissions, central Europe fails to achieve the long-term air quality guideline value, but the influence of climate change is small.

The influence of climate change under RCP 8.5 on achieving the WHO guidelines and interim targets for annual short-term exposure over London is shown in Table 1. Averaged over London, the 99th percentile MDA8 value increases by 3 $\mu\text{g m}^{-3}$ in the future (Table 1). For both periods, the first interim target is achieved, but the second interim target and the air quality guideline for short-term exposure are not met. Considering the 10-year periods, the first interim target is not met on ~2 days, on average, while the air quality guideline is not met on about 20 days for both present-day and future.



Table 1: Short-term 99th percentile values of MDA8 O₃, and 24-hour mean PM_{2.5} and NO₂ calculated annually from hourly data for the respective present-day and future 10-year periods for each of the 56 locations over London. Mean values across all 56 locations are given in the 2nd column. The WHO short-term averaging period interim target and air quality guideline (AQG) values (WHO 2021) are shown in bold. Exceedance days per year are calculated over the full 10-year period and divided by 10 to estimate exceedance days per year for the WHO interim target values and the relevant air quality guideline value (rightmost column). The spatial variation in exceedance days across the 56 locations are represented by the standard deviation.

		Exceedance days for different targets (days per year)					
		MDA8/ 24-hour mean (µg m ⁻³)	160	120			100
O ₃	Interim target/AQG	160	120				100
	PD	127.6	1.5±0.9	7.8±4.7			18.0±8.9
	Future	130.8	1.7±1.1	7.7±4.7			17.8±9.8
PM _{2.5}	Interim target/AQG	75	50	37.5	25	15	
	PD	42.1	0.1±0.1	1.4±1.2	7.7±4.0	33.5±12.8	97.2±27.1
	Future	48.3	0.5±0.3	4.6±1.8	14.5±5.1	43.2±14.1	110.8±30.1
NO ₂	Interim target/AQG	120	50				25
	PD	124.5	17.0±32.4	183.7±92.7			305.7±56.5
	Future	147.8	24.8±36.9	200.5±84.9			313.4±50.4

The 99th percentile of 24-hour mean surface PM_{2.5} concentrations averaged over London suggest that the first and second interim targets are achieved for both time periods (Table 1). The number of exceedance days of the PM_{2.5} air quality guidelines increases from ~97 days for present-day to ~111 days in the future. For NO₂, the 99th percentile values averaged over London increase from 125 to 148 µg m⁻³ between present-day and future; both values exceed the first interim target for short-term NO₂ exposure (Table 1). The air quality guideline is exceeded on ~306 days for present day and ~313 days in the future 10-year periods, with differences in exceedances of ~50 days over the different London locations for both periods. Hence, for the three air pollutants, the short-term air quality guideline values are not met for present-day or in the future when utilising 2012 anthropogenic emissions in these simulations.

6. Conclusions

Climate change alone is likely to worsen O₃ and PM_{2.5} air quality over much of continental Europe but improve O₃ air quality over parts of northern Europe including the UK. This study uses an innovative coupled and nested approach to determine the importance of key processes in governing the responses of surface ozone (O₃), fine particulate matter (PM_{2.5}) and nitrogen dioxide (NO₂) to climate change in the 21st century across a range of spatial scales: the continental scale across Europe, regional scale across the UK and at the street scale across London. The one-way nested WRF-EMEP4UK regional



atmospheric chemistry transport model (50 km × 50 km resolution over Europe; 5 km × 5 km over the UK) is driven by climate change projections from the Representative Concentration Pathway (RCP) 8.5 from the UK Earth System Model 645 HadGEM2-ES, which produces annual-mean temperature increases exceeding 4°C across Europe. The regional WRF-EMEP4UK model is coupled to the street-scale ADMS-Urban model. This methodology allows for a consistent assessment of the impacts of large-scale climate change on air quality to be simulated over Europe, the UK and in London.

Changes in O₃ and PM_{2.5} over Europe due to a large climate change signal show good agreement with previous findings using RCP8.5 or SSP3-7.0. There is a strong contrast in the summer and winter-mean O₃ responses to climate change.

650 Surface O₃ decreases (up to 8 ppbv) in winter over most of Europe, and in summer, large O₃ increases are found over southern Europe (up to 10 ppbv) but O₃ reductions occur over northern Europe. Lower hemispheric background O₃ levels are highlighted as the driver of future O₃ decreases over northern Europe in numerous studies (e.g., Colette et al. 2015; Turnock et al. 2022). In addition, higher NO_x concentrations in winter over parts of northern Europe under climate change, lead to greater titration of O₃ by NO reducing surface O₃ levels. Larger O₃ dry deposition velocities and a higher mixing layer may 655 also contribute to winter surface O₃ decreases. Higher temperatures lead to a doubling of natural biogenic isoprene emissions in summer over Europe, and this likely dominates the increases in summer O₃ in southern Europe. Reductions in O₃ dry deposition in summer may also contribute to summer surface O₃ increases. This O₃ increase has been referred to as the O₃ climate penalty (e.g., Wu et al. 2008; Colette et al. 2015). However, these simulations do not consider the posited CO₂ inhibition effect on isoprene emissions or represent detailed isoprene nitrate chemistry. The size of the O₃ climate penalty 660 remains uncertain because of uncertainty in the magnitude of isoprene and monoterpene emissions and their sensitivity to climate and associated atmospheric CO₂ and vegetation changes and the interplay of these factors (e.g., Lin et al. 2016).

Annual-average surface PM_{2.5} concentrations increase by 5–10 µg m⁻³ (up to 30%) over most of Europe by the 2090s. This increase is also driven by higher biogenic isoprene and monoterpene emissions, promoting secondary organic aerosol (SOA) formation, most notably in summer. Changes in climate-sensitive biogenic emissions are the dominant driver of both surface 665 O₃ and PM_{2.5} responses to climate change in summer over continental Europe in this study; therefore, uncertainties in biogenic emission processes represents a major limitation for the findings of this study.

Increased wintertime precipitation over Central Europe promotes more wet deposition of sulphur dioxide (SO₂) which reduces sulphate aerosol loadings in the 2090s; a similar but much smaller response is found for nitrate. For both species, increases in dry deposition of SO_x (SO₂+SO₄) and oxidised nitrogen in winter are prominent across Europe. Primary organic matter also shows larger changes in winter with increases over emission source locations. Summer responses of inorganic 670 and primary organic matter PM_{2.5} components are more muted. Wind-driven increases in sea-salt aerosol are found over much of Atlantic whilst Saharan dust transported to Europe is reduced. However, the impact of climate change on dust is highly uncertain due to uncertainties in changes to meteorological and soil properties. Winter increases in mixing layer height over Central Europe also influence surface O₃, NO_x and, via sulphate, PM_{2.5} levels.



675 Over the UK, the spatial patterns and magnitudes of O₃, PM_{2.5} and NO₂ responses to climate change simulated over the UK domain at 5 km × 5 km resolution are similar to those simulated at 50 km × 50 km resolution over the European domain, suggesting that our results are not strongly sensitive to model resolution.

Examining the seasonality of urban air pollution across London, the O₃ peak amplitude is reduced in the 2090s under climate change. In contrast, PM_{2.5} and NO₂ concentrations exhibit a more pronounced wintertime peak. For all air pollutants, the
680 urban model simulates substantially greater spatial variability than the regional model over London due to its representation of local concentration gradients close to road sources. The diurnal cycle of urban O₃ for London in winter is flatter and in summer displays a shift towards higher morning and lower afternoon values under climate change. Higher PM_{2.5} and NO₂ levels and reduced diurnal variability are found in both seasons in the future, with larger night-time increases evident in winter. Whilst monthly mean NO₂ magnitudes are ~10% higher at the street scale using ADMS-Urban compared to the
685 regional EMEP4UK model, both models show consistent responses to climate change for all three air pollutants.

The changes in O₃, PM_{2.5} and NO₂ concentrations under climate change have implications for achieving the 2021 WHO long and short-term air quality guidelines in the 2000s and 2090s under RCP8.5. For peak season (April-September) maximum daily 8-hour (MDA8) surface O₃, whilst much of Europe meets the first interim target of 100 µgm⁻³, the air quality guideline of 60 µg m⁻³ is exceeded except in parts of northern Europe in the present-day. While the reduction in hemispheric
690 background O₃ due to climate change benefits attainment of these guidelines in northern Europe, it hinders attainment elsewhere in Europe. Hence, under this high warming scenario, without concurrent emission reductions, WHO air quality guidelines for peak season O₃ will be even more challenging to meet, except in parts of northern Europe. Annual-average PM_{2.5} concentrations meet the first and second interim targets for much of Europe. Very limited areas of northern Europe meet the stringent WHO guidelines for annual mean PM_{2.5} of 5 µg m⁻³ for present-day. Under climate change alone, this
695 target will be extremely difficult to meet. However, Turnock et al (2022) showed that implementing future O₃ precursor emission reductions alongside climate change mitigation reduced exceedances of both these long-term WHO air quality guideline values across the globe. The long-term air quality guidelines of annual-average NO₂ ≤ 10 µg m⁻³ are viable for much of Europe for present-day and, despite climate-induced changes in NO_x, remain unaltered in the future. Considering short-term air quality guidelines over London, whilst the first interim target is achieved for the 99th percentile values of
700 MDA8 O₃ and 24-hour mean PM_{2.5}, it is not for 24-hour mean NO₂. None of these air pollutants met the short-term air quality guidelines for present-day or future under this climate change scenario and fixed 2012 anthropogenic emissions.

This study finds that robust projections of the magnitude of the impact of climate change on surface O₃ and PM_{2.5} for Europe crucially rely on accurate representation of climate-sensitive biogenic emissions. Climate driven changes in dry and wet deposition and mixing layer height also have an important influence on surface O₃ and PM_{2.5} concentrations. Changes in
705 other climate-sensitive natural emissions sources including lighting and wildfires are neglected in these simulations; wildfires in particular, are likely to become a much more important source in the future. Whilst the focus of the model simulations is to isolate the climate change response, the assumption of present-day levels for anthropogenic emissions, atmospheric methane and CO₂ concentrations means the chemical environment and the resulting atmospheric chemistry

kinetics and atmospheric composition changes would be different if emission changes under RCP8.5 (or another
710 scenario/pathway) were also employed. Notably, large methane increases projected for high warming RCP8.5 and SSP3-7.0 scenarios would substantially increase background O₃ levels (by ~50%; Turnock et al. 2022). Therefore, both emissions and climate change need to be considered in relation to future mitigation policies.

Whilst horizontal resolution effects are found to be less relevant for calculations of long-term WHO air quality guidelines, for short-term guidelines, and in particular for attainment of NO₂ air quality guidelines, high resolution and explicit
715 representation of its emission sources are crucial. However, it is noted, that these results are based on one climate scenario and present-day anthropogenic emissions, which is a major caveat of this study. Dynamical downscaling studies to achieve finer spatial representation of atmospheric composition change, as presented here, limit the use of multiple models with ensemble members that would be required for a comprehensive quantification of uncertainties (scenario, structural, internal
720 climate variability) related to climate change. Such high-resolution projections are largely only available from climate models, such as CORDEX at the regional-scale for Europe or UKCP18 at the local-scale for the UK, but these do not include projections of atmospheric composition. New variable resolution modelling capabilities will enhance two-way nested high-resolution simulation of future atmospheric composition, but extension to the urban street-scale remains challenging, despite its importance for air quality guideline assessment and for health effects. Nevertheless, this study adds to the evidence that although parts of northern Europe may benefit from lower hemispheric background O₃, strong future mitigation measures
725 will need to be implemented for continental Europe to meet the ambitious WHO air quality guidelines, especially for short-term exposure, in the future.

7. Appendix A: Additional Figures and tables

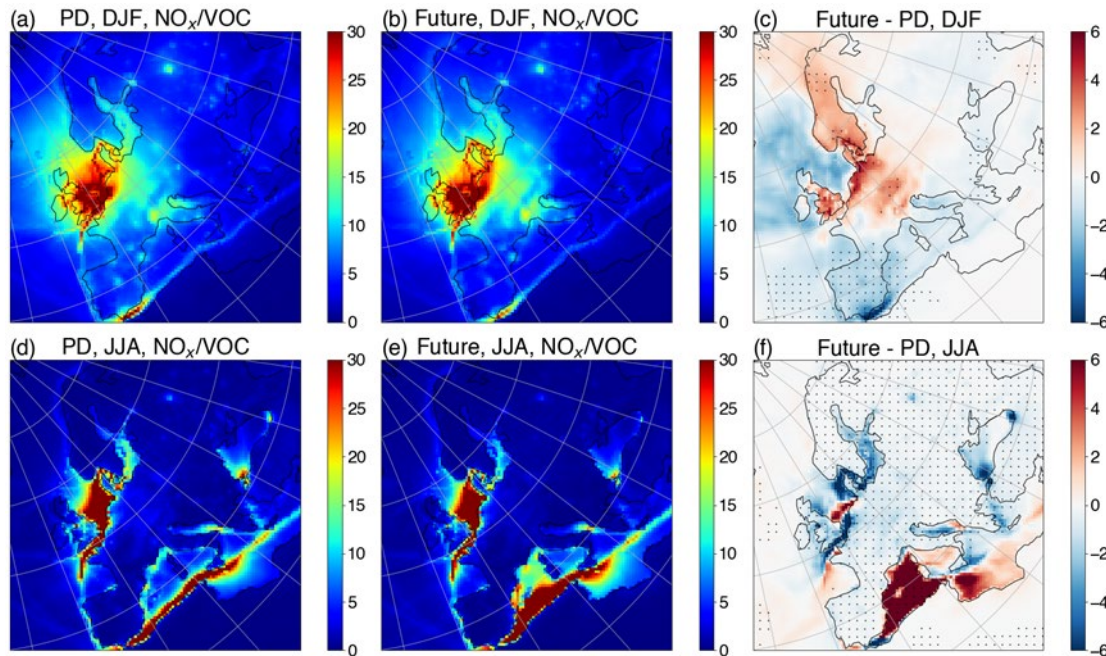


Figure A1: Surface NO_x/VOC mixing ratios as indicators of O₃ chemical environments for present day (1996-2005) in a) winter and d) summer, and for future (2090-2099) in b) winter and e) summer and differences in chemical environments between future and present-day in c) winter and f) summer. VOC concentrations are represented as the sum of isoprene (C₅H₈) and formaldehyde (HCHO).

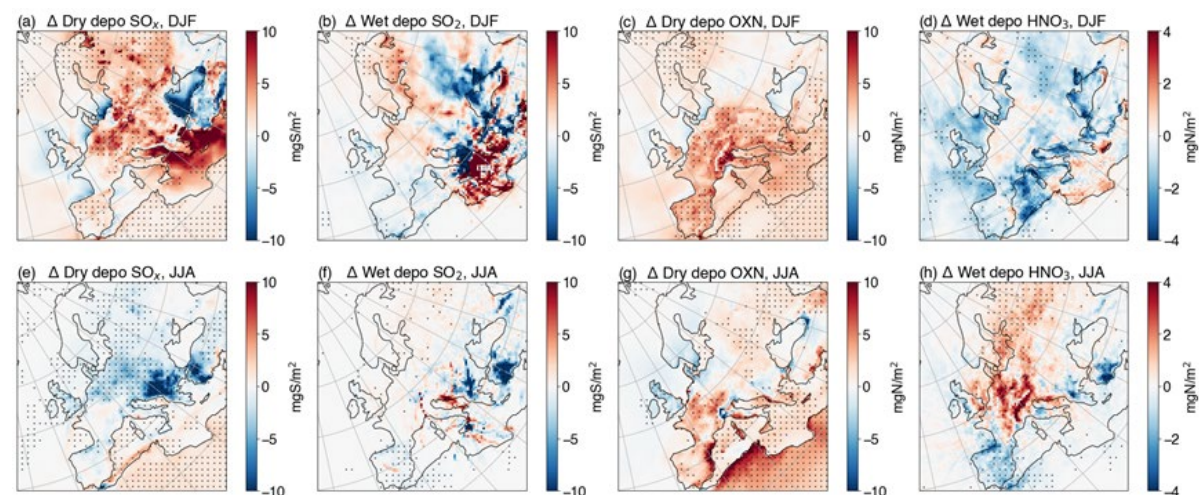


Figure A2. Differences in dry deposition of SO_x (SO₂+SO₄) in a) winter, e) summer, in wet deposition of SO₂ in c) winter, f) summer, in dry deposition of oxidised Nitrogen (largely HNO₃) in c) winter and g) summer and in wet deposition of HNO₃ in d) winter and h) summer between present day (1996-2005) and future (2090-99).

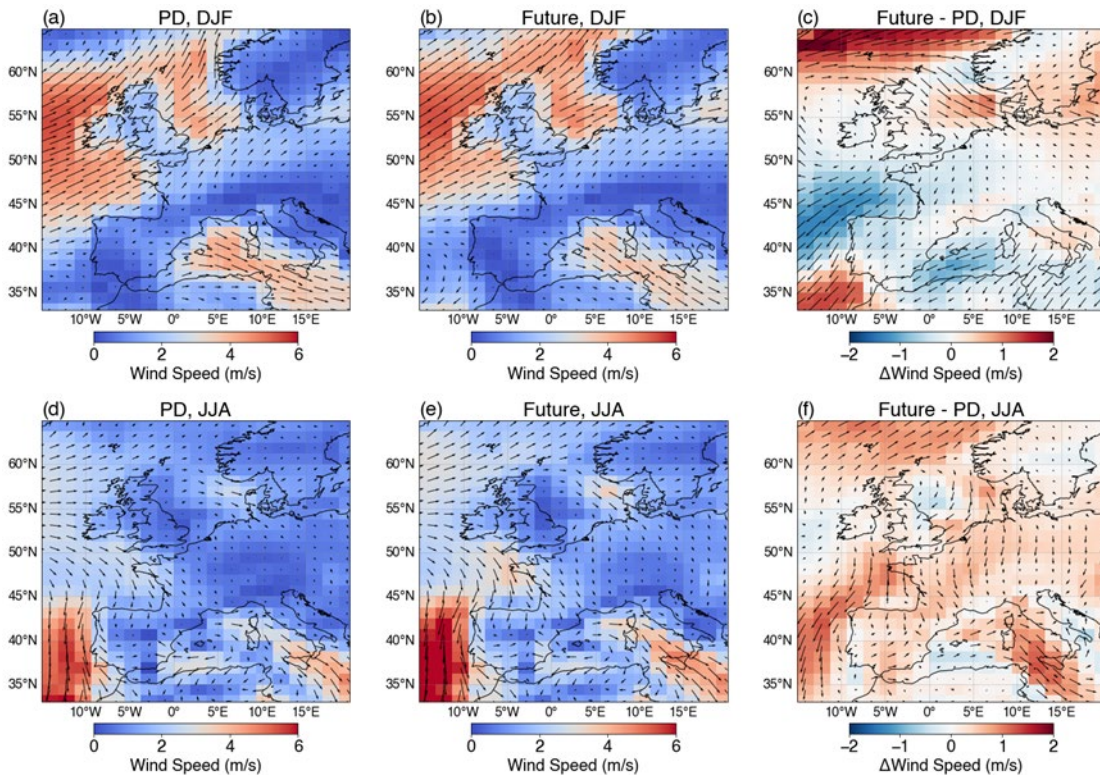


Figure A3: Wind speed and directions (uas, vas) for present day (1996-2005) for a) winter, d) summer and for future (2090-2099) for c) winter and e) summer and differences between present-day and future for e) winter and f) summer from the HadGEM2-ES model. Model outputs from WRF-EMEP4UK were not available for U and V winds, but 6-hourly nudging propagates this climate change signal across the WRF-EMEP4UK model domains.

740

745

750



755 **Table A1: Winter and summer mean O₃ (ppbv), PM_{2.5} (µg m⁻³) and NO₂ (ppbv) concentrations simulated over the UK at 50 × 50 km and 5 × 5 km resolution averaged over the whole UK, and North (above 54°N) and South (below 54°N) UK.**

DJF		O₃	PM_{2.5}	NO₂
50 × 50 km: All UK/North/South				
UK	PD	42.6/47.9/38.7	12.3/8.3/15.3	17.8/11.3/22.6
	Future	37.4/42.9/33.4	13.2/8.7/16.5	18.7/11.0/24.4
5 × 5 km: All UK/North/South				
UK	PD	43.8/48.2/40.6	10.9/7.7/13.2	17.2/11.7/21.2
	Future	38.7/43.4/35.2	11.5/7.9/14.1	18.0/11.2/23.0
JJA		O₃	PM_{2.5}	NO₂
50 × 50 km: All UK/North/South				
UK	PD	48.1/47.2/48.7	7.1/5.6/8.3	8.1/3.7/11.3
	Future	45.3/41.8/47.8	7.0/5.3/8.3	8.2/3.4/11.7
5 × 5 km: All UK/North/South				
UK	PD	50.1/49.2/50.7	6.2/4.9/7.2	7.5/3.6/10.3
	Future	46.9/43.6/49.4	6.1/4.6/7.2	7.5/3.3/10.6

760

765

770



Table A2: Median monthly values over London for surface O₃ (ppbv), PM_{2.5} (µg m⁻³) and NO₂ (ppbv) concentrations for present-day (PD) and future from the EMEP4UK 5 × 5 km UK domain (10 grid-boxes) and from the ADMS-Urban (56 receptor locations) models. Month 1= January etc.

Month			1	2	3	4	5	6	7	8	9	10	11	12
O ₃	PD	EMEP4UK	9.9	13.5	22.6	29.0	29.9	28.6	23.2	20.2	15.2	10.7	7.8	10.0
		ADMS	9.8	13.4	21.2	28.3	28.5	27.3	22.6	18.7	14.6	10.1	7.6	9.4
	Future	EMEP4UK	9.4	10.9	18.4	24.4	28.2	26.7	24.0	21.3	16.1	8.9	4.8	6.7
		ADMS	9.0	10.3	17.4	22.8	26.7	25	22.1	19.6	14.8	8.2	4.5	6.5
PM _{2.5}	PD	EMEP4UK	15.8	16.0	10.4	9.7	8.6	9.7	7.2	7.5	8.9	15.1	21.0	15.8
		ADMS	14.0	13.6	11.2	9.7	8.3	9.0	7.5	7.5	9.0	14.4	18.8	13.8
	Future	EMEP4UK	14.6	17.3	10.6	10.1	7.7	9.4	8.1	7.7	11.7	17.6	26.3	18.4
		ADMS	13.6	16.0	10.3	10	7.8	9.4	8.2	8.0	11.8	17.3	24.4	16.9
NO ₂	PD	EMEP4UK	25.8	26.0	20.7	18.1	18.3	17.5	14.8	18.7	22.7	28.6	29.7	27.9
		ADMS	30.0	29.5	25.8	22.6	21.7	20.6	18.4	22.6	26.5	32.4	33.7	32.5
	Future	EMEP4UK	26.6	30.0	23.5	20.9	17.1	15.8	16.2	18.3	25.7	35.2	35.1	30.7
		ADMS	31.2	34.7	26.9	25.2	20.8	19.9	20.3	22.9	30.2	38.6	39.8	34.9

Data availability

775 Model outputs from simulations performed in this study are available on request to the corresponding authors. Data for wind fields were obtained from the CMIP5 data archive, which is hosted at the Earth System Grid Federation and is freely available to download from <https://esgf-node.llnl.gov/search/cmip5/> (last access: 12 December 2025).

Author contributions

780 RMD, ZL, MV and OW conceptualised the research study. The main formal analysis was conducted by ZL, RMD and OW with inputs from MV, FMO'C, STT, with the figures created by ZL. MV, CMH and JRS developed the coupled model aided by FMO'C. Funding acquisition was led by RMD, aided by DEH, MRH and contributions from LKW, JRS and DJC. RMD and ZL prepared the manuscript aided by OW with contributions from STT and FMO'C. All co-authors reviewed and edited the manuscript.

Competing interests

785 One co-author is a member of the editorial board of Atmospheric Chemistry and Physics. The other co-authors declare that they have no conflict of interest.



Disclaimer

Copernicus Publications adds a standard disclaimer: “Copernicus Publications remains neutral with regard to jurisdictional claims made in the text, published maps, institutional affiliations, or any other geographical representation in this paper.

790 While Copernicus Publications makes every effort to include appropriate place names, the final responsibility lies with the authors. Views expressed in the text are those of the authors and do not necessarily reflect the views of the publisher.”

Acknowledgements

We thank David Simpson for providing EMEP MSC-W model code and Ian MacKenzie for his contribution to the coupled model development and performing model simulations, and James Weber for insightful discussions. This work used the

795 ARCHER UK National Supercomputing Service.

Financial support

The model simulations were supported by funding under the UK Natural Environment Research Council via grants: NE/M003906/1 and NE/M002381/1. Zhenze Liu thanks the National Natural Science Foundation of China (NSFC), the

Natural Science Foundation of Jiangsu Province and the China Postdoctoral Science Foundation for funding under grants

800 42307140, SBK2023043946 and 2023M731749. FMO'C was supported by the Met Office Hadley Centre Climate Programme funded by DSIT. The contributions of Steven Turnock were funded by the Met Office Climate Science for

Service Partnership (CSSP) China project under the International Science Partnerships Fund (ISPF).

Review statement

The review statement will be added by Copernicus Publications listing the handling editor as well as all contributing referees

805 according to their status anonymous or identified.

References

Air Quality Expert Group (AQEG): Ozone in the UK – Recent Trends and Future Projections, https://uk-air.defra.gov.uk/library/reports?report_id=1064, 2021.

Allen, R. J., Hassan, T., Randles, C. A., and Su, H.: Enhanced land–sea warming contrast elevates aerosol pollution in a

810 warmer world, *Nat. Clim. Change*, 9, 300–305, <https://doi.org/10.1038/s41558-019-0401-4>, 2019.

Andersson, C., and Engardt, M.: European ozone in a future climate: Importance of changes in dry deposition and isoprene emissions, *J. Geophys. Res.*, 115, D02303, <https://doi.org/10.1029/2008JD011690>, 2010.



Allen, R. J., Landuyt, W., and Rumbold, S. T.: An increase in aerosol burden and radiative effects in a warmer world, *Nat. Clim. Change*, 6, 269–274, <https://doi.org/10.1038/nclimate2827>, 2016.

815 Arneth, A., Schurgers, G., Hickler, T., and Miller, P.: Effects of species composition, land surface cover, CO₂ concentration and climate on isoprene emissions from European forests, *Plant Biology*, 10, 150–162, <https://doi.org/10.1055/s-2007-965247>, 2008.

Athanassiadou, M., Baker, J., Carruthers, D., Collins, W., Girnary, S., Hassell, D., Hort, M., Johnson, C., Johnson, K., Jones, R., Thomson, D., Trought, N., and Witham, C. S.: An assessment of the impact of climate change on air quality at two UK sites, *Atmos. Environ.*, 44, 1877–1886, <https://doi.org/10.1016/j.atmosenv.2010.02.024>, 2010.

820 Banks, A., Kooperman, G. J., and Xu, Y.: Meteorological influences on anthropogenic PM_{2.5} in future climates: Species level analysis in the Community Earth System Model v2, *Earth's Future*, 10, e2021EF002298, <https://doi.org/10.1029/2021EF002298>, 2022.

Berglen, T. F., Berntsen, T. K., Isaksen, I. S. A., and Sundet, J. K.: A global model of the coupled sulfur/oxidant chemistry 825 in the troposphere: The sulfur cycle, *J. Geophys. Res.*, 109, D19310, <https://doi.org/10.1029/2003JD003948>, 2004.

Bergström, R., Denier van der Gon, H. A. C., Prévôt, A. S. H., Yttri, K. E., and Simpson, D.: Modelling of organic aerosols over Europe (2002–2007) using a volatility basis set (VBS) framework: application of different assumptions regarding the formation of secondary organic aerosol, *Atmos. Chem. Phys.*, 12, 8499–8527, <https://doi.org/10.5194/acp-12-8499-2012>, 2012.

830 Carruthers, D. J., Holroyd, R. J., Hunt, J. C. R., Weng, W. S., Robins, A. G., Apsley, D. D., Thomson, D. J., and Smith, F. B.: UK-ADMS: a new approach to modelling dispersion in the Earth's atmospheric boundary layer, *J. Wind Eng. Ind. Aerodyn.*, 52, 139–153, [https://doi.org/10.1016/0167-6105\(94\)90044-2](https://doi.org/10.1016/0167-6105(94)90044-2), 1994.

Colette, A., Andersson, C., Baklanov, A., Bessagnet, B., Brandt, J., Christensen, J. H., Doherty, R. M., Engardt, M., Geels, C., Giannakopoulos, G., Hedegaard, G. B., Katragkou, E., Langner, J., Lei, H., Manders, A., Melas, D., Meleux, F., Rouïl, 835 L., Sofiev, M., Soares, J., Stevenson, D. S., Tombrou-Tzella, M., Varotsos, K. V., and Young, P. J., et al.: Is the ozone climate penalty robust in Europe?, *Environ. Res. Lett.*, 10, 084015, <https://doi.org/10.1088/1748-9326/10/8/084015>, 2015.

Collins, W. J., Bellouin, N., Doutriaux-Boucher, M., Gedney, N., Halloran, P., Hinton, T., Hughes, J., Jones, C. D., Joshi, M., Liddicoat, S., Martin, G., O'Connor, F., Rae, J. G. L., Senior, C. A., Sitch, S., Totterdell, I., Wiltshire, A., and Woodward, S.: Development and evaluation of an Earth-system model – HadGEM2, *Geosci. Model Dev.*, 4, 1051–1075, 840 <https://doi.org/10.5194/gmd-4-1051-2011>, 2011.

Collins, W. J., Lamarque, J.-F., Schulz, M., Boucher, O., Eyring, V., Hegglin, M. I., Maycock, A., Myhre, G., Prather, M., Shindell, D., and Smith, S. J.: AerChemMIP: quantifying the effects of chemistry and aerosols in CMIP6, *Geosci. Model Dev.*, 10, 585–607, <https://doi.org/10.5194/gmd-10-585-2017>, 2017.

Dawson, J. P., Adams, P. J., and Pandis, S. N.: Sensitivity of PM_{2.5} to climate in the eastern US: a modeling case study, 845 *Atmos. Chem. Phys.*, 7, 4295–4309, <https://doi.org/10.5194/acp-7-4295-2007>, 2007.



Doherty, R. M., Heal, M. R., and O'Connor, F. M.: Climate change impacts on human health over Europe through its effect on air quality, *Environ. Health*, 16, 118, <https://doi.org/10.1186/s12940-017-0325-2>, 2017.

Doherty, R. M., O'Connor, F. M., and Turnock, S. T.: Projections of future air quality are uncertain, but which source of uncertainty is most important?, *J. Geophys. Res.-Atmos.*, 127, e2022JD037948, <https://doi.org/10.1029/2022JD037948>, 2022.

850 Doherty, R. M., Wild, O., Shindell, D. T., Zeng, G., MacKenzie, I. A., Collins, W. J., Fiore, A. M., Stevenson, D. S., Dentener, F. J., Schultz, M. G., Hess, P., Derwent, R. G., and Keating, T. J.: Impacts of climate change on surface ozone and intercontinental ozone pollution: a multi-model study, *J. Geophys. Res.-Atmos.*, 118, 3744–3763, <https://doi.org/10.1002/jgrd.50266>, 2013.

855 Emberson, L.: Effects of ozone on agriculture, forests and grasslands, *Philos. Trans. R. Soc. A Math. Phys. Eng. Sci.*, 378(2183), 20190327, <https://doi.org/10.1098/rsta.2019.0327>, 2020.

ENTEC: Defra UK ship emissions inventory, final report, available at: http://uk-air.defra.gov.uk/reports/cat15/1012131459_21897_Final_Report_291110.pdf, 2010.

Finney, D., Doherty, R., Wild, O., Stevenson, D., MacKenzie, I., and Blyth, A. M.: A projected decrease in lightning under 860 climate change, *Nat. Clim. Change*, 8, 210–213, <https://doi.org/10.1038/s41558-018-0072-6>, 2018.

Fiore, A. M., Milly, G. P., Hancock, S. E., Quiñones, L., Bowden, J. H., Helstrom, E., Lamarque, J.-F., Schnell, J., West, J. J., and Xu, Y.: Characterizing changes in eastern U.S. pollution events in a warming world, *J. Geophys. Res.-Atmos.*, 127, e2021JD035985, <https://doi.org/10.1029/2021JD035985>, 2022.

865 Fiore, A. M., Naik, V., Spracklen, D. V., Steiner, A., Unger, N., Prather, M., Bergmann, D., Cameron-Smith, P. J., Cionni, I., Collins, W. J., Dalsøren, S., Eyring, V., Folberth, G. A., Ginoux, P., Horowitz, L. W., Josse, B., Lamarque, J.-F., MacKenzie, I. A., Nagashima, T., O'Connor, F. M., Righi, M., Rumbold, S. T., Shindell, D. T., Skeie, R. B., Sudo, K., Szopa, S., Takemura, T., and Zeng, G.: Global air quality and climate, *Chem. Soc. Rev.*, 41, 6663–6683, <https://doi.org/10.1039/C2CS35095E>, 2012.

Fu, T. M., and Tian, H.: Climate change penalty to ozone air quality: review of current understandings and knowledge gaps, 870 *Curr. Pollut. Rep.*, 5, 159–171, <https://doi.org/10.1007/s40726-019-00115-6>, 2019.

Gomez, J., Allen, R. J., Turnock, S. T., Horowitz, L. W., Tsigaridis, K., Bauer, S. E., Olivié, D., Thomson, E. S., and Ginoux, P.: The projected future degradation in air quality is caused by more abundant natural aerosols in a warmer world, *Commun. Earth Environ.*, 4, 22, <https://doi.org/10.1038/s43247-023-00688-7>, 2023.

Greater London Authority (GLA) 2013. London Atmospheric Emissions Inventory (LAEI): 875 <https://data.london.gov.uk/dataset/london-atmospheric-emissions-inventory-2010>, last access: 7 December 2017.

Hamilton, I. G., Stocker, J., Evans, S., Davies, M., and Carruthers, D.: The impact of the London Olympic Parkland on the urban heat island, *J. Build. Perform. Simul.*, 7, 119–132, <https://doi.org/10.1080/19401493.2013.791343>, 2014.



Hood, C., MacKenzie, I. A., Stocker, J., Johnson, K., Carruthers, D., Vieno, M., and Doherty, R. M.: Air quality simulations for London using a coupled regional-to-local modelling system, *Atmos. Chem. Phys.*, 18, 11221–11245, 880 <https://doi.org/10.5194/acp-18-11221-2018>, 2018.

Jacob, D. J., and Winner, D. A.: Effect of climate change on air quality, *Atmos. Environ.*, 43, 51–63, <https://doi.org/10.1016/j.atmosenv.2008.09.051>, 2009.

Johnson, C. E., Collins, W. J., Stevenson, D. S., and Derwent, R. G.: Relative roles of climate and emissions changes on future tropospheric oxidant concentrations, *J. Geophys. Res.-Atmos.*, 104, 18631–18645, 885 <https://doi.org/10.1029/1999JD900204>, 1999.

Jones, C. D., Hughes, J. K., Bellouin, N., Hardiman, S. C., Jones, G. S., Knight, J., Liddicoat, S., O'Connor, F. M., Andres, R. J., Bell, C., Boo, K.-O., Bozzo, A., Butchart, N., Cadule, P., Corbin, K. D., Doutriaux-Boucher, M., Friedlingstein, P., Gornall, J., Gray, L., Halloran, P. R., Hurt, G., Ingram, W. J., Lamarque, J.-F., Law, R. M., Meinshausen, M., Osprey, S., Palin, E. J., Parsons Chini, L., Raddatz, T., Sanderson, M. G., Sellar, A. A., Schurer, A., Valdes, P., Wood, N., Woodward, 890 S., Yoshioka, M., and Zerroukat, M.: The HadGEM2-ES implementation of CMIP5 centennial simulations, *Geosci. Model Dev.*, 4, 543–570, <https://doi.org/10.5194/gmd-4-543-2011>, 2011.

Kirtman, B., S.B. Power, J.A. Adedoyin, G.J. Boer, R. Bojariu, I. Camilloni, F.J. Doblas-Reyes, A.M. Fiore, M. Kimoto, G.A. Meehl, M. Prather, A. Sarr, C. Schär, R. Sutton, G.J. van Oldenborgh, G. Vecchi and H.J. Wang, 2013: Near-term Climate Change: Projections and Predictability. In: *Climate Change 2013: The Physical Science Basis. Contribution of Working Group I to the Fifth Assessment Report of the Intergovernmental Panel on Climate Change*, edited by Stocker, T.F., D. Qin, G.-K. Plattner, M. Tignor, S.K. Allen, J. Boschung, A. Nauels, Y. Xia, V. Bex and P.M. Midgley., Cambridge University Press, Cambridge, United Kingdom and New York, NY, USA. https://www.ipcc.ch/site/assets/uploads/2018/02/WG1AR5_Chapter11_FINAL.pdf

Lacressonnière, G., Foret, G., Beekmann, M. et al. Impacts of regional climate change on air quality projections and 900 associated uncertainties. *Climatic Change* 136, 309–324, <https://doi.org/10.1007/s10584-016-1619-z>, 2016.

Lacressonnière, G., Peuch, V.-H., Vautard, R., Arteta, J., Déqué, M., Joly, M., Josse, B., Marécal, V., and Saint-Martin, D.: European air quality in the 2030s and 2050s: Impacts of global regional emission trends and of climate change, *Atmos. Environ.*, 92, 348–358, <https://doi.org/10.1016/j.atmosenv.2014.04.033>, 2014.

Lamarque, J.-F., Bond, T. C., Eyring, V., Granier, C., Heil, A., Klimont, Z., Lee, D., Liousse, C., Mieville, A., Owen, B., 905 Schultz, M. G., Shindell, D., Smith, S. J., Stehfest, E., Van Aardenne, J., Cooper, O. R., Kainuma, M., Mahowald, N., McConnell, J. R., Naik, V., Riahi, K., and van Vuuren, D. P.: Historical (1850–2000) gridded anthropogenic and biomass burning emissions of reactive gases and aerosols: methodology and application, *Atmos. Chem. Phys.*, 10, 7017–7039, <https://doi.org/10.5194/acp-10-7017-2010>, 2010.

Langner, J., Engardt, M., Baklanov, A., Christensen, J. H., Gauss, M., Geels, C., Hedegaard, G. B., Nuterman, R., Simpson, 910 D., Soares, J., Sofiev, M., Wind, P., and Zakey, A.: A multi-model study of impacts of climate change on surface ozone in Europe, *Atmos. Chem. Physics*, 12, 10423–10440, <https://doi.org/10.5194/acp-12-10423-2012>, 2012.



Lin, C., Heal, M. R., Vieno, M., MacKenzie, I. A., Armstrong, B. G., Butland, B. K., Milojevic, A., Chalabi, Z., Atkinson, R. W., Stevenson, D. S., Doherty, R. M., and Wilkinson, P.: Spatiotemporal evaluation of EMEP4UK-WRF v4.3 atmospheric chemistry transport simulations of health-related metrics for NO₂, O₃, PM₁₀, and PM_{2.5} for 2001–2010, *Geosci. Model Dev.*, 10, 1767–1787, <https://doi.org/10.5194/gmd-10-1767-2017>, 2017

Lin, G., Penner, J. E., and Zhou, C.: How will SOA change in the future?, *Geophys. Res. Lett.*, 43, 1718–1726, <https://doi.org/10.1002/2015GL067137>, 2016.

Liu, J., Wang, X., Wu, D., Ji, M., Wei, H., and Li, Y.: Historical footprints and future projections of global dust burden from bias-corrected CMIP6 models, *npj Clim. Atmos. Sci.*, 7, 1, <https://doi.org/10.1038/s41612-023-00550-9>, 2024.

Lu, X., Zhang, L., and Shen, L.: Meteorology and climate influences on tropospheric ozone: a review of natural sources, chemistry, and transport patterns, *Curr. Pollut. Rep.*, 5, 238–260, <https://doi.org/10.1007/s40726-019-00118-3>, 2019.

Malkin, T. L., Heard, D. E., Hood, C., Stocker, J., Carruthers, D., MacKenzie, I. A., Doherty, R. M., Vieno, M., Lee, J., Kleffmann, J., Laufs, S., and Whalley, L. K.: Assessing chemistry schemes and constraints in air quality models used to predict ozone in London against the detailed Master Chemical Mechanism, *Faraday Discuss.*, 189, 589–616, <https://doi.org/10.1039/C5FD00218D>, 2016.

Meinshausen, M., Smith, S. J., Calvin, K., Daniel, J. S., Kainuma, M. L. T., Lamarque, J.-F., Matsumoto, K., Montzka, S. A., Raper, S. C. B., Riahi, K., Thomson, A., Velders, G. J. M., and van Vuuren, D. P.: The RCP greenhouse gas concentrations and their extensions from 1765 to 2500, *Climatic Change*, 109, 213–241, <https://doi.org/10.1007/s10584-011-0156-z>, 2011.

Met Office Hadley Centre (MOHC) (2012): WCRP CMIP5: Met Office Hadley Centre (MOHC) HadGEM2-ES model output collection, Centre for Environmental Data Analysis, <https://catalogue.ceda.ac.uk/uuid/216becee8a6844ba8f8f98b9f075a635>, 2012.

Murphy, J. M., Harris, G. R., Sexton, D. M. H., Kendon, E. J., Bett, P. E., Clark, R. T., Eagle, K. E., Fosser, G., Fung, F., Lowe, J., McDonald, R. E., McInnes, R. N., McSweeney, C. F., Mitchell, J. F. B., Rostron, J. W., Thornton, H. E., Tucker, S., and Yamazaki, K.: UKCP18 aiLand Projections: Science Report, Met Office, available at: <https://www.metoffice.gov.uk/pub/data/weather/uk/ukcp18/science-reports/UKCP18-Land-report.pdf>, 2018.

Ots, R., Young, D. E., Vieno, M., Xu, L., Dunmore, R. E., Allan, J. D., Coe, H., Williams, L. R., Herndon, S. C., Ng, N. L., Hamilton, J. F., Bergström, R., Di Marco, C., Nemitz, E., Mackenzie, I. A., Kuenen, J. J. P., Green, D. C., Reis, S., and Heal, M. R.: Simulating secondary organic aerosol from missing diesel-related intermediate-volatility organic compound emissions during the Clean Air for London (ClearfLo) campaign, *Atmos. Chem. Phys.*, 16, 6453–6473, <https://doi.org/10.5194/acp16-6453-2016>, 2016.

Park, I. H., and Yeh, S. W.: Projections of the North Atlantic warming hole can be constrained using ocean surface density as an emergent constraint, *Commun. Earth Environ.*, 5, 98, <https://doi.org/10.1038/s43247-024-01269-y>, 2024.



945 Pye, H. O. T., Liao, H., Wu, S., Mickley, L. J., Jacob, D. J., Henze, D. K., and Seinfeld, J. H.: Effect of changes in climate and emissions on future sulfate-nitrate-ammonium aerosol levels in the United States, *J. Geophys. Res.-Atmos.*, 114, D01205, <https://doi.org/10.1029/2008JD010701>, 2009.

Racherla, P. N., and Adams, P. J.: Sensitivity of global tropospheric ozone and fine particulate matter concentrations to climate change, *J. Geophys. Res.-Atmos.*, 111, D24103, <https://doi.org/10.1029/2005JD006939>, 2006.

950 The Royal Society (RS): Effects of net-zero policies and climate change on air quality, The Royal Society, ISBN: 978-1-78252-558-5, available at: <https://royalsociety.org/-/media/policy/projects/air-quality/air-quality-and-climate-change-report.pdf>, 2021.

Schnell, J. L., Prather, M. J., Josse, B., Naik, V., Horowitz, L. W., Zeng, G., Shindell, D. T., and Faluvegi, G.: Effect of climate change on surface ozone over North America, Europe, and East Asia, *Geophys. Res. Lett.*, 43, 3509–3518, <https://doi.org/10.1002/2016GL068060>, 2016.

955 Shindell, D. T., Faluvegi, G., Koch, D. M., Schmidt, G. A., Unger, N., and Bauer, S. E.: Improved attribution of climate forcing to emissions, *Science*, 326, 716–718, <https://doi.org/10.1126/science.1174760>, 2009.

Silva, R. A., West, J. J., Lamarque, J.-F., Shindell, D. T., Collins, W. J., Faluvegi, G., Folberth, G. A., Horowitz, L. W., Nagashima, T., Naik, V., Rumbold, S. T., Sudo, K., Takemura, T., Bergmann, D., Cameron-Smith, P., Doherty, R. M., Josse, B., MacKenzie, I. A., Stevenson, D. S., and Zeng, G.: Future global mortality from changes in air pollution attributable to climate change, *Nat. Clim. Change*, 7, 647–651, <https://doi.org/10.1038/nclimate3354>, 2017.

960 Simpson, D., Benedictow, A., Berge, H., Bergström, R., Emberson, L. D., Fagerli, H., Flechard, C. R., Hayman, G. D., Gauss, M., Jonson, J. E., Jenkin, M. E., Nyíri, A., Richter, C., Semeena, V. S., Tsyro, S., Tuovinen, J.-P., Valdebenito, Á., and Wind, P.: The EMEP MSC-W chemical transport model – technical description, *Atmos. Chem. Phys.*, 12, 7825–7865, <https://doi.org/10.5194/acp-12-7825-2012>, 2012.

965 Simpson, D., Tsyro, S., and Wind, P.: Updates to the EMEP/MSC-W model, in: Transboundary particulate matter, photo-oxidants, acidifying and eutrophying components. EMEP Status Report 1/2015, The Norwegian Meteorological Institute, Oslo, Norway, 129–138, www.emep.int, 2015.

Smith, S. E., Stocker, J., Seaton, M., and Carruthers, D.: Model inter-comparison and validation study of ADMS plume 970 chemistry schemes. *Int. J. Environ. Pollut.*, 62, 395–406, <https://www.inderscienceonline.com/doi/abs/10.1504/IJEP.2017.089427>, 2017.

Stocker, J., Hood, C., Carruthers, D., and McHugh, C.: ADMS-Urban: developments in modelling dispersion from the city scale to the local scale, *Int. J. Environ. Pollut.*, 50, 308–316, <https://www.inderscienceonline.com/doi/abs/10.1504/IJEP.2012.051202>, 2012.

975 Taylor, K. E., Stouffer, R. J., and Meehl, G. A.: An overview of CMIP5 and the experiment design, *Bull. Am. Meteorol. Soc.*, 93, 485–498, <https://doi.org/10.1175/BAMS-D-11-00094.1>, 2012.



Thornhill, G. D., Collins, W., Olivié, D., Skeie, R. B., Archibald, A., Bauer, S. E., Riva, R., Sanderson, M. G., et al.: Climate-driven chemistry and aerosol feedbacks in CMIP6 Earth system models, *Atmos. Chem. Phys.*, 21, 1105–1126, <https://doi.org/10.5194/acp-21-1105-2021>, 2021.

980 Turnock, S. T., Allen, R. J., Andrews, M., Bauer, S. E., Deushi, M., Emmons, L., Good, P., Horowitz, L., John, J. G., Michou, M., Nabat, P., Naik, V., Neubauer, D., O'Connor, F. M., Olivié, D., Oshima, N., Schulz, M., Sellar, A., Shim, S., Takemura, T., Tilmes, S., Tsigaridis, K., Wu, T., and Zhang, J.: Historical and future changes in air pollutants from CMIP6 models, *Atmos. Chem. Phys.*, 20, 14547–14579, <https://doi.org/10.5194/acp-20-14547-2020>, 2020.

Turnock, S. T., Allen, R., Archibald, A. T., Dalvi, M., Folberth, G. A., Griffiths, P. T., Keeble, J., Robertson, E., and 985 O'Connor, F. M.: The future climate and air quality response from different near-term climate forcer, climate, and land-use scenarios using UKESM1, *Earth's Future*, 10, e2022EF002687, <https://doi.org/10.1029/2022EF002687>, 2022.

Venkatram, A., Karamchandani, P., Pai, P., and Goldstein, R.: The development and application of a simplified ozone modeling system (SOMS), *Atmospheric Environment*, 28(22), 3665–3678, [https://doi.org/10.1016/1352-2310\(94\)00190-V](https://doi.org/10.1016/1352-2310(94)00190-V), 1994.

990 Vieno, M., Dore, A. J., Stevenson, D. S., Doherty, R., Heal, M. R., Reis, S., Hallsworth, S., Tarrason, L., Wind, P., Fowler, D., Simpson, D., and Sutton, M. A.: Modelling surface ozone during the 2003 heat-wave in the UK, *Atmos. Chem. Phys.*, 10, 7963–7978, <https://doi.org/10.5194/acp-10-7963-2010>, 2010.

Vieno, M., Heal, M. R., Hallsworth, S., Famulari, D., Doherty, R. M., Dore, A. J., Tang, Y. S., Braban, C. F., Leaver, D., Sutton, M. A., and Reis, S.: The role of long-range transport and domestic emissions in determining atmospheric secondary 995 inorganic particle concentrations across the UK, *Atmos. Chem. Phys.*, 14, 8435–8447, <https://doi.org/10.5194/acp-14-8435-2014>, 2014.

Vieno, M., Heal, M. R., Williams, M. L., Carnell, E. J., Nemitz, E., Stedman, J. R., and Reis, S.: The sensitivities of emissions reductions for the mitigation of UK PM_{2.5}, *Atmos. Chem. Phys.*, 16, 265–276, <https://doi.org/10.5194/acp-16-265-2016>, 2016.

1000 Watson, L. A., Shallcross, D. E., Utembe, S. R., and Jenkin, M. E.: A Common Representative Intermediates (CRI) mechanism for VOC degradation, Part 2: Gas phase mechanism reduction, *Atmos. Environ.*, 42, 7196–7204, <https://doi.org/10.1016/j.atmosenv.2008.07.034>, 2008.

West, J. J., Smith, S. J., Silva, R. A., Naik, V., Zhang, Y., Adelman, Z., Fry, M. M., Anenberg, S. C., Horowitz, L. W., and Lamarque, J.-F.: Co-benefits of mitigating global greenhouse gas emissions for future air quality and human health, *Nat. Clim. Change*, 3, 885–889, <https://doi.org/10.1038/nclimate2009>, 2013.

World Health Organization: WHO global air quality guidelines: particulate matter (PM_{2.5} and PM₁₀), ozone, nitrogen dioxide, sulfur dioxide and carbon monoxide, World Health Organization, Geneva, ISBN 9789240034228, <https://www.who.int/publications/i/item/9789240034228>, 2021.



Wu, S., Mickley, L. J., Leibensperger, E. M., Jacob, D. J., Rind, D., and Streets, D. G.: Effects of 2000–2050 global change on ozone air quality in the United States, *J. Geophys. Res.: Atmos.*, 113, D06302, <https://doi.org/10.1029/2007JD008917>, 2008.

Young, P. J., Archibald, A. T., Bowman, K. W., Lamarque, J.-F., Naik, V., Stevenson, D. S., Tilmes, S., Voulgarakis, A., Wild, O., Bergmann, D., Cameron-Smith, P., Cionni, I., Collins, W. J., Dalsøren, S. B., Doherty, R. M., Eyring, V., Faluvegi, G., Horowitz, L. W., Josse, B., Lee, Y. H., MacKenzie, I. A., Nagashima, T., Plummer, D. A., Righi, M., Rumbold, S. T., Skeie, R. B., Shindell, D. T., Strode, S. A., Sudo, K., Szopa, S., and Zeng, G.: Pre-industrial to end 21st century projections of tropospheric ozone from the Atmospheric Chemistry and Climate Model Intercomparison Project (ACCMIP), *Atmos. Chem. Phys.*, 13, 2063–2090, <https://doi.org/10.5194/acp-13-2063-2013>, 2013.

Zanis, P., Akritidis, D., Turnock, S., Naik, V., Szopa, S., Georgoulias, A. K., Bauer, S. E., Deushi, M., Horowitz, L. W., Keeble, J., Le Sager, P., O'Connor, F. M., Oshima, N., Tsigaridis, K., and van Noije, T.: Climate change penalty and benefit on surface ozone: A global perspective based on CMIP6 Earth system models, *Environ. Res. Lett.*, 17(2), 024014, <https://doi.org/10.1088/1748-9326/ac4a34>, 2022.

Zeng, G., and Pyle, J. A.: Changes in tropospheric ozone between 2000 and 2100 modeled in a chemistry-climate model, *Geophys. Res. Lett.*, 30(7), 1392, <https://doi.org/10.1029/2002GL016708>, 2003. Air Quality Expert Group (2021) Ozone in the UK – Recent Trends and Future Projections. UK Department for Environment, Food and Rural Affairs, London. 1025 PB14701. https://uk-air.defra.gov.uk/library/reports?report_id=1064.